AGU PUBLICATIONS

Water Resources Research

RESEARCH ARTICLE
10.1002/2014WR015924

Key Points:
- Univariate regression misrepresents the scaling behavior of daily streamflow
- Inverse moments represent the lower half of the distribution of streamflow
- Increasing scale reduces the variability of streamflow in the study region

Correspondence to:
W. H. Farmer,
william.farmer@tufts.edu

Citation:
Farmer, W. H., T. M. Over, and R. M. Vogel (2015), Multiple regression and inverse moments improve the characterization of the spatial scaling behavior of daily streamflows in the Southeast United States, *Water Resour. Res.*, *51*, doi:10.1002/2014WR015924.

Received 29 MAY 2014
Accepted 9 FEB 2015
Accepted article online 13 FEB 2015

Multiple regression and inverse moments improve the characterization of the spatial scaling behavior of daily streamflows in the Southeast United States

William H. Farmer[1,3], Thomas M. Over[2], and Richard M. Vogel[3]

[1]U.S. Geological Survey, Reston, Virginia, USA, [2]U.S. Geological Survey, Urbana, Illinois, USA, [3]Department of Civil and Environmental Engineering, Tufts University, Medford, Massachusetts, USA

Abstract Understanding the spatial structure of daily streamflow is essential for managing freshwater resources, especially in poorly gaged regions. Spatial scaling assumptions are common in flood frequency prediction (e.g., index-flood method) and the prediction of continuous streamflow at ungaged sites (e.g. drainage-area ratio), with simple scaling by drainage area being the most common assumption. In this study, scaling analyses of daily streamflow from 173 streamgages in the southeastern United States resulted in three important findings. First, the use of only positive integer moment orders, as has been done in most previous studies, captures only the probabilistic and spatial scaling behavior of flows above an exceedance probability near the median; negative moment orders (inverse moments) are needed for lower streamflows. Second, assessing scaling by using drainage area alone is shown to result in a high degree of omitted-variable bias, masking the true spatial scaling behavior. Multiple regression is shown to mitigate this bias, controlling for regional heterogeneity of basin attributes, especially those correlated with drainage area. Previous univariate scaling analyses have neglected the scaling of low-flow events and may have produced biased estimates of the spatial scaling exponent. Third, the multiple regression results show that mean flows scale with an exponent of one, low flows scale with spatial scaling exponents greater than one, and high flows scale with exponents less than one. The relationship between scaling exponents and exceedance probabilities may be a fundamental signature of regional streamflow. This signature may improve our understanding of the physical processes generating streamflow at different exceedance probabilities.

1. Introduction

Since rivers and streams are the main sources of freshwater for human use, the responsible development and management of these resources relies on a sound understanding of their behavior in space and time. An understanding of streamflow behavior is essential to a wide range of projects, from water supply planning and flood management to hydropower development and irrigation scheduling. One of the key attributes of regional streamflow is its spatial scaling behavior, which arises from the relationship between climatic inputs and watershed-integrated streamflow as mediated by the properties of the region's watersheds. Understanding, evaluating and interpreting spatial scaling behavior is the focus of this study; in doing so we have identified some important impacts of methodology on the results of scaling analysis, and once corrected, identified a fundamental scaling behavior.

The spatial scaling behavior of streamflow captures the relationship between river discharge and the interactions of streamflow-generating process in the contributing upstream area. This behavior is often characterized by a scale-transformation function $h(\ldots)$. The scale-transformation function transforms streamflow at two sites, i and j, such that they exhibit distributional equality:

$$Q_i \stackrel{d}{=} h(\ldots)Q_j \tag{1}$$

where Q_i and Q_j represent the contemporaneous streamflows at the two sites and $h(\ldots)$ is the scale-transformation function. In the consideration of spatial scaling, $h(\ldots)$ is assumed to be a simple function of the respective drainage areas, A_i and A_j (as in *Vogel and Sankarasubramanian* [2000], as well as numerous other researchers).

The definition of spatial scaling further distinguishes between regions or networks that exhibit "simple-scaling" and "multiscaling" processes. In both cases, the scale-transformation function takes the form of

$$h(\ldots)=h(A_i,A_j)=\left[\frac{A_i}{A_j}\right]^{\beta} \tag{2}$$

where β is commonly referred to as the spatial scaling exponent. Under simple-scaling processes, the spatial scaling exponent β is constant across the distribution of streamflow for a given region or network of streams [*Gupta and Waymire*, 1990; *Smith*, 1992]. In the case of multiscaling, this exponent varies with the exceedance probability of the streamflows of interest. In other words, in the case of multiscaling, streamflows with different exceedance probabilities have different scaling exponents.

In one of the most common applications of spatial scaling, upstream contributing drainage area is used to transfer streamflow information from a set of gaged sites to an ungaged site of interest. This technique is referred to as the "drainage-area ratio" (DAR) method for prediction in ungaged basins as in *Farmer and Vogel* [2013]. The DAR method assumes that the discharge per unit area (specific discharge) is constant across both a geographic region of interest and the distribution of streamflows and thus is, in terms of probability distributions, equivalent to simple scaling with a unit exponent. Such an assumption implies that the specific discharge across two sites is equivalent.

The drainage area is often the basin characteristic that has the widest range of values in a given region, covering three or more orders of magnitude. Therefore, variations in drainage area exponent, especially deviations from one, can cause substantial differences in estimated discharges. We argue in this paper that scaling exponents for high flows are significantly less than one and those for low flows are significantly greater than one in our study region and similar hydroclimatic regions. Consider a numerical example where the ratio of the drainage area of two basins in a given region is 10. Now, if the high-flow scaling exponent, say at the 0.01 exceedance probability, is 0.7, then the ratio of quantiles is $10^{0.7}=5.00$ rather than 10, as would be obtained from a straight drainage-area ratio (DAR) approach. At the same time if the low-flow exponent, say at an exceedance probability of 0.99, is 1.5, then the ratio of quantiles is $10^{1.5}=31.6$. In such a case, the larger basin would have small high-flow quantiles, relative to the DAR, but large low-flow quantiles. Furthermore, on the basis of flow-per-unit-area, the larger basin would have a thinner-tailed probability distribution of streamflows and a less flashy hydrograph, with lower peaks and longer recessions, as would be expected. We also want to establish what scaling behavior is observed in the study region as a basis for developing hypotheses regarding the underlying hydrological processes and for other possible uses such as evaluating hydrological model output across a range of scales.

Spatial scaling behavior also underlies the assumptions of hydrologic homogeneity associated with the index-flood method [*Dalrymple*, 1960]. This method assumes a common regional probability distribution of floods, after rescaling with an "index flood." The index flood is usually taken to be the mean annual flood and is traditionally estimated based on basin characteristics, such as the drainage area and precipitation. The assumption of a common regional probability distribution after rescaling implies a constant regional coefficient of variation (CV). As others have shown, a constant regional CV is also implied by the presence of simple scaling when the flood distribution depends on drainage area alone [*Gupta and Waymire*, 1990; *Smith*, 1992; *Gupta et al*., 1994; *Vogel and Sankarasubramanian* 2000; *Yue and Wang*, 2004; *Yue and Gang*, 2009]. While the presence of simple scaling can be used to assess the presence of this regional probability distribution, *Dalrymple* [1960] introduces a separate metric to assess the regional homogeneity of the index flood.

Previous investigators have sought to identify well-behaved, homogenous regions suitable for the application of techniques like the index-flood method [*Skaugen and Vaeringstad*, 2005]. Because of the practical importance of the problem, most research on spatial scaling has focused on flood flows [*Gupta and Waymire*, 1990; *Smith*, 1992; *Gupta et al*., 1994, 1996; *Dawdy and Gupta*, 1995; *Gupta and Dawdy*, 1995; *Pandey*, 1998; *Eaton et al*., 2002; *Yue and Gan*, 2009; *Ishak et al*., 2011]. Additionally, some studies have examined the scaling behavior of mean annual flows: *Vogel and Sankarasubramanian* [2000] found that U.S. mean annual flows exhibited simple scaling while *Yue and Gan* [2004] and *Buttle and Eimers* [2009] reached similar conclusions with respect to flows in Canada. *Vogel and Kroll* [1990, 1992], *Furey and Gupta* [2000], *Yue and Wang* [2004], and *Modarres* [2010] explored the spatial scaling of low flows. While most research focuses on the spatial scaling of a particular range of flow statistics, we consider the full range of daily streamflows.

In general, there are two types of methods for assessing the spatial scaling behavior of streamflow: (1) using product or probability weighted moments [*Pandey*, 1998; *Yue and Gan*, 2004] and (2) using quantiles [*Singh*, 1971; *Gupta et al*., 1994; *Gupta and Dawdy*, 1995; *Over et al*., 2014]. These methods are typically executed with a regression analysis relating each moment or quantile to drainage area. Additionally, breaking regions into smaller or more-homogeneous areas leads to an improved goodness of fit for the spatial scaling behavior of flows [*Yue and Gan*, 2009]; the definition of such regions can dramatically affect the interpretation of scaling behavior. In such cases, differences in scaling behavior are explained by variations in climate or other basin characteristics not explicitly considered [*Yue and Wang*, 2004; *Glaster*, 2007; *Yue and Gan*, 2009]. For high flows, the majority of studies reviewed here found drainage-area scaling exponents ranging from 0.7 to 0.8 or even lower.

We are unaware of any previous research on the spatial scaling of streamflows that has considered the scaling of moments with negative moment orders. Such moments, representing the positive-order moments of the inverse of the data set, are known as inverse moments. The consideration of negative moment orders is standard in the nonlinear physics literature [e.g., *Halsey et al*., 1986], and negative moments have been considered in principle in the analysis of river flow time series in a multifractal framework [e.g., *Tessier et al*., 1996]. We will show that the consideration of inverse moments is essential to capturing the full range of scaling behavior.

Typical of the wider literature, the studies reviewed for this work almost exclusively considered drainage area alone when examining scaling behavior [*Yue and Gan*, 2004; *Yue and Wang*, 2004, among others], though some studies consider, at most, one or two other explanatory variables, including precipitation [*Modarres*, 2010] and rainfall intensities and stream density [*Ishak et al*., 2011]. *Ishak et al*. [2011] considered other variables, but found them to be insignificant. Even if the goal is to understand how streamflow scales with drainage area, excluding other variables in regression analyses can lead to significant confusion or misinterpretation. Multiple regression can be used to capture the variations in basin characteristics that drive scaling behavior. The omission of relevant variables, if correlated with drainage area, results in biased and inconsistent estimates of scaling exponents.

Spatial scaling behavior is closely linked with the development of regional hydrologic models for the prediction of various streamflow statistics. In the field of hydrology, there is a long and rich history of the development of regional hydrologic models quantifying the relationship between basin characteristics and streamflows statistics in a multiple regression framework. Such regressions typically rely heavily on the explanatory power of the drainage area ratio and can be interpreted as an application of spatial scaling behavior. One example of this is the U.S. Geological Survey's National Streamflow Statistics Program, which has developed regional regression relationships for the prediction of a wide range of streamflow statistics. These regional regressions exist for all regions of the U.S. and rely on watershed characteristics [see *Ries III*, 2007]. The work presented here has direct applicability to the development and improvement of such multivariate regional hydrologic models.

The primary goal of this study is to improve our understanding of the spatial scaling behavior of daily streamflow. We consider two important elements of scaling analysis: (1) ensuring that the full range of streamflow scaling behavior is captured in an analysis of moments and (2) illuminating the consequences of neglecting additional explanatory variables. We are less concerned with the distinction between simple scaling and multiscaling and more concerned with improving our understanding of scaling behavior and the insights it provides on streamflow-generating processes. In particular, we observe that, once additional explanatory variables are added, low flows scale with exponents greater than one and high flows scale with exponents less than one. In support of what would be expected, this finding implies that larger basins have less variable streamflow than smaller basins. A better understanding of scaling behavior will lead to an enhanced ability to estimate daily flow time series at ungaged sites and, subsequently, an improved ability to manage water resources.

The next section of this paper presents a brief summary of scaling analysis and a description of the data used in this study. This discussion is followed by an exploration of the relationship between streamflow moments and quantiles, demonstrating the limitations in previous analyses of the scaling behavior of moments. Through a series of regression analyses, we show that considering only the explanatory power of drainage area can lead to biased and inconsistent estimates of scaling exponents, resulting in a

misinterpretation of spatial scaling behavior. These analyses lead to an improved understanding of spatial scaling behavior and its implications for understanding the spatial variability of streamflow and streamflow-generating processes at different scales.

2. Methods and Background

2.1. Moment Analysis

The use of product moments of streamflow is a common technique for assessing the spatial scaling behavior of streamflows; this approach is referred to herein as "moment analysis." In moment analysis, the same spatial scaling exponent from *Eq*. (1) and (2) is used to relate the r^{th} product moment of the streamflows in two basins:

$$E\left[Q_i^r\right] = \left[\frac{A_i}{A_j}\right]^{r\beta_r} E\left[Q_j^r\right] \tag{3}$$

where $E\left[Q_i^r\right] = \int_0^\infty Q_i^r f(Q_i) dQ_i$, with $f(Q_i)$ being the probability density function (pdf) of daily flows at site i, and β_r is the scaling exponent for the r^{th} moment. Equation (3) can be simplified by considering site j to be a reference site with a unit drainage area so that

$$E\left[Q_i^r\right] = A_i^{r\beta_r} E\left[Q_*^r\right] \tag{4}$$

where $E\left[Q_*^r\right]$ is the r^{th} moment of streamflow at the unit-area reference gage. Note that, having been divided by a unit area, drainage area A_i is now unitless. Taking the logarithms of this simplification leads to the linear function:

$$\ln\left(E\left[Q_i^r\right]\right) = \alpha_r + r\beta_r \ln\left(A_i\right) \tag{5}$$

where $\alpha_r = \ln(E\left[Q_*^r\right])$. The constant α_r and the slope $r\beta_r$ for each moment order r can then be estimated by applying least-squares regression to the moments and drainage areas within a region. Each site in a region may have a different length of record so that longer records may provide more accurate representations of the moments. This heteroscedasticity can be accounted for, at least approximately, by using weighted least-squares (WLS) regression with at-site record lengths weighting each observation. Under simple scaling, the scaling exponent β_r will be constant across moment orders, so that the slope estimates are a linear function of moment order, r. This linearity is assessed by evaluating the goodness-of-fit of the resulting linear model: $b_r = r\beta_r$, for which most studies have only considered positive integer moment orders, though there is no reason to limit r to that set.

Because of the simple scaling relationship $b_r = r\beta_r$, evidence of significant curvature in the function b_r, whether concave or convex [*Gupta and Waymire*, 1990], is indicative of multiscaling, whereas a good linear fit without significant curvature and a zero intercept is emblematic of simple scaling [see e.g., *Vogel and Sankarasubramanian*, 2000]. Concave curvature in b_r indicates decreasing variability with increasing scale, whereas convex curvature indicates increasing variability with scale [*Gupta et al*., 1994]. In most studies of streamflow, when significant deviations from linearity in b_r are observed, they have been convex for positive moment orders [*Gupta and Waymire*, 1990], though the results of *Smith* [1992] for peak flows in Appalachia suggest the presence of increasing variability with scale for small drainage basins (less than 50 km^2) along with decreasing variability with scale for large drainage basins. Illustrative examples of the process of moment analysis can be found in *Pandey* [1998] and *Vogel and Sankarasubramanian* [2000].

This product-moment-based approach to moment analysis is limited in that it does not estimate the scaling exponent β_r directly. Instead, the quantity $r\beta_r$ is estimated; the scaling exponent β_r can then be assessed by dividing the quantity by the moment order or by applying a linear regression to the slope estimates. Alternatively, β_r can be directly estimated by considering power averages instead of power moments. *Jensen* [1998] provides background on the power means and averages, the latter being an estimator of the former. The power mean is the r^{th} root of the r^{th} moment. Using power mean here is equivalent to taking the r^{th} root of equation (4):

$$\left(E\left[Q_i^r\right]\right)^{1/r} = A_i^{\beta_r} \left(E\left[Q_*^r\right]\right)^{1/r}, \tag{6}$$

which can be linearized by taking logarithms as

$$\ln\left(\left(E\left[Q_i^r\right]\right)^{1/r}\right)=\alpha_r{}'+\beta_r\ln\left(A_i\right). \tag{7}$$

Here $\alpha'_r=\ln\left(\left(E\left[Q_*^r\right]\right)^{1/r}\right)$ represents the natural logarithm of the r^{th} power mean for the reference basin with a unit drainage area. The same process of WLS regression can then be applied to equation (7), providing a direct estimate of the scaling exponent β_r. Under certain assumptions described in Appendix A, the quantity $A_i^{\beta_r}$ can be formally thought of as the effective contributing drainage area ratio at the given moment order. $A_i^{\beta_r}$ indicates the ratio, at moment order r, of the effective contributing drainage area at scale A_i to the effective contributing drainage area at the unit-area reference basin.

With sample data, the power mean can be approximated with the power average [*Jensen*, 1998]. For a site with N days of observation, the r^{th} product moment is estimated as

$$m_r=\frac{1}{N}\sum_{i=1}^{N}Q_i^r. \tag{8}$$

Using a similar formulation, the power mean can be estimated as the power average, $\tilde{m}_r$. The power average is estimated as the r^{th} root of the estimated product moment

$$\tilde{m}_r=\sqrt[r]{m_r}=\sqrt[r]{\frac{1}{N}\sum_{i=1}^{N}Q_i^r}. \tag{9}$$

Conveniently for calculation, it has been shown that the power average reduces to the geometric mean for $r=0$ [*Jensen*, 1998]. (In addition, the power average reduces to the harmonic mean for $r=-1$ and the arithmetic mean when $r=1$, as shown in *Jensen* [1998].)

2.2. Quantile Analysis

Quantile analysis provides a similar assessment, but is conducted, when applied to continuous streamflow measurements, using quantiles of the flow duration curve (FDC) rather than moments. Analogous to equations (4) and (5), for each exceedance probability, p, the site i can be compared against a reference site such that

$$Q_{i,p}=A_i^{\beta_p}Q_{*,p} \tag{10}$$

which, as with moment analysis, can be linearized as

$$\ln\left(Q_{i,p}\right)=\ln(Q_{*,p})+\beta_p\ln\left(A_i\right). \tag{11}$$

where p is the probability that a daily flow exceeds that streamflow quantile, $Q_{*,p}$ is the pth percentile of streamflow at the unit-area reference gage, and β_p is the scaling exponent for that exceedance probability. Analogous to the moment-based effective contributing drainage area ratio $A_i^{\beta_r}$ discussed previously, $A_i^{\beta_p}$ can be thought of as the effective contributing drainage area ratio at the exceedance probability p. (See Appendix A.) Under simple scaling, β_p is constant and does not depend on p. Representation of theoretical multiscaling models in terms of quantiles is not straightforward, though *Gupta et al.* [1994] have given a first-order approximation to the quantile representation of a class of multiscaling models. This first-order approximation shows that the usual case of decreasing drainage area exponent β with decreasing p (larger floods) corresponds to the concave case of β_r, indicating decreasing variability with increasing scale.

2.3. Connecting Moments and Quantiles

As discussed, the spatial scaling behavior of streamflow in a region can be evaluated by considering either the moments or quantiles of streamflow. In practice, it is not clear how to assess the agreement between these two methods because it is not clear how to map the exceedance probabilities of a flow series to their moment. To our knowledge, the only general point of comparison between moments and quantiles is the correspondence between the geometric mean ($r=0$) and the median ($p=0.5$) for any logarithmically symmetric distribution (e.g. lognormal).

In light of this situation, we employ the following approximate approach. We assume that an exceedance probability and a moment order correspond if the quantile and moment agree in magnitude after reconciling units by using power averages. The power averages were computed for several moment orders in each

basin. Within each basin, the moment order of each power average was assumed to correspond to the exceedance probability of the quantile having a magnitude most similar to the power average.

2.4. Handling Omitted Variable Bias

Although an attractive theoretical approach is to define a hydrologically homogeneous region as one in which the distribution of daily streamflow depends only on drainage area (as *Gupta et al*. [1994] did for peak flow), to date no general method of finding such regions has been developed. Therefore, in practice drainage area cannot be assumed to be the only variable affecting streamflow generation within a given region, and it is incomplete to assess the scaling behavior of streamflow with only the explanatory power of drainage area. In particular, using drainage area alone when assessing scaling may result in a statistical phenomenon known as omitted-variable bias (OVB).

A common concern in econometrics and other applications of multivariate statistics, OVB arises when independent variables not included in a multiple regression model are correlated with both the independent variable of interest (here, drainage area) and with the dependent variable. OVB results in biased and inconsistent estimates of regression parameters. This implies that unless a region is known to be homogeneous in the sense defined by *Gupta et al*. [1994], little faith can be placed in the regression estimates of streamflow scaling exponents generated from regression on drainage area alone. Appendix B provides a theoretical derivation of OVB and a discussion of its consequences in a simple case. The occurrence of OVB implies that valuable information about the watersheds in the gaged network is ignored and such information could impact the interpretation of the spatial scaling behavior of streamflow. We hypothesize that accounting for these confounding variables with a more rigorous multiple-regression framework may mitigate OVB and provide a more effective approach for assessing the spatial scaling behavior of streamflow.

To test for the presence of OVB, the moment and quantile analyses were conducted with regression on drainage area alone. The same analysis was then conducted with a multiple-regression formulation of equation (5)

$$\ln\left(\left(E\left[Q_i^r\right]\right)^{1/r}\right)=\delta_{r,0}+\delta_{r,1}\ln\left(A_i\right)+\delta_{r,2}\ln\left(X_{1,i}\right)+\delta_{r,3}\ln\left(X_{2,i}\right)+\ldots \tag{12}$$

where the *X*s are additional watershed explanatory variables such as average precipitation, temperature, soil composition, etc. For each moment or quantile, stepwise regression was used to select a subset of relevant variables. Using an F-test, the model that resulted in the fewest parameters without causing us to reject the null hypothesis (all other variables having coefficients of zero) was selected as the most parsimonious model to avoid overfitting. It is shown that excluding these variables in heterogeneous regions results in a biased and inconsistent estimate of the spatial scaling exponent.

3. Description of Data Sources

Daily streamflow and basin characteristics were derived from U.S. Geological Survey (USGS) streamgages in the southeastern United States, mainly in Alabama and Georgia. Reference-quality gages from the USGS database of Geospatial Attributes of Gages for Evaluating Streamflow, Version 2 (GAGES-II) [*Falcone*, 2011] in the region were supplemented with gages from previous USGS studies of rural flood frequency. The supplemental gages were screened by the responsible USGS Water Science Centers (WSCs) and found to be free of major human impacts, especially in the case of flood flows. (Human impacts were defined as substantial withdrawals, discharges, and regulation. Further information can be obtained by referring to the classification of reference-quality gages in the GAGES-II database [*Falcone*, 2011].) The resulting list of sites was circulated through the WSCs to screen out any additional gages that were subject to substantial regulation or substantial land-use changes. The result was a collection of 182 streamgages that contained reliable records of natural streamflow for at least 10 years between 1 October 1980, and 30 September 2010. For the present study, the collection of 182 gages was further refined to include only the 173 stations with no zero-flow days to avoid complications in logarithmic operations. The removal of gages with zero-flow days would undoubtedly result in bias if the results of this study were used for regional predictions, but that is not its purpose here.

Daily streamflow data were downloaded from the USGS National Water Information System Web Interface (NWIS Web: http://waterdata.usgs.gov/nwis). When available, basin characteristics for each site, including

soil composition, drainage area, and average climate conditions, were extracted from the GAGES-II database [*Falcone*, 2011]. For those sites that were not part of the GAGES-II database, basin characteristics were developed from the source data cited by GAGES-II. A full list of variables considered here is presented in Table 1.

4. The Connection Between Quantiles and Moment Orders

The relation between exceedance probabilities and moment orders for the study region was mapped for each site by interpolating the power average, for each moment r, along the empirical, at-site, daily flow duration curve to obtain the associated exceedance probability of that moment order. This process was conducted for moment orders ranging from $r = -10$ to 10; increments of 1 were used from -10 to -5 and from 5 to 10 and increments of 0.05 were used from -5 to 5. Moments of a negative order are known as inverse moments, representing the normal moments of the inverse of the data set. The median results of this mapping, as well as the 5th and 95th percentiles of each moment order, across all sites are shown in Figure 1.

From Figure 1, positive moment orders only capture the behavior of the streamflows above the median (approximately), which corresponds to exceedance probabilities below 50%. The general correspondence of positive moments to higher flows is expected because exponentiation of any data set to a power greater than unity magnifies the effect of the larger values in the set; for any $0 < r < 1$, the effect of larger values relative to the smaller ones is less than when $r = 1$, but it is still larger, whereas for $r = 0$ (at which point the power average corresponds to the geometric mean), all values have the same effect on the power mean in the sense that a proportional change in one has the same effect as a change of the same proportion in any. As noted above, an exact correspondence of the geometric mean and the median occurs for any distribution that is symmetric when transformed logarithmically, such as lognormal. Therefore, to the extent that daily streamflow can be approximated by a lognormal or other exponentiated symmetric distribution, the correspondence of the zeroth moment order to the median in Figure 1 is not surprising. In general, Figure 1 shows that basing a scaling analysis on positive integer moments considers only the scaling behavior of flows greater than some moderate value probably near the median.

The full range of exceedance probabilities of the flows is only captured by considering both positive and negative moment orders. Since the reciprocal of a data set exaggerates the magnitude of the smaller numbers, it is not surprising that the inverse moments capture the lower tail of the probability distribution. As seen by the width of the 90% interval, the mapping of inverse moments is much more variable among the different gage records than that of positive moments, a fact that may have practical implications for understanding low-flow scaling behavior. In addition, there is a degree of asymmetry in the mapping between the positive and negative moment orders: for positive moment orders, the extremum of the high-flow exceedance probabilities (the value 0) is reached at a much smaller absolute moment order than is the extremum of the low-flow exceedance probabilities (i.e., the value 1). This result indicates that the positive power averages become dominated by the largest data value at a relatively small absolute moment order, whereas the negative power averages require a larger absolute moment order to become similarly dominated. This results from the high-flow tail of the probability distributions of daily flows being fatter than the low-flow tail. Further implications of the shape of this curve are being investigated.

The mapping between exceedance probabilities and moment orders will also prove useful in comparing conclusions reached by quantile analysis to those reached by moment analysis; note that the mean ($r = 1$) has a median exceedance probability of about 28%.

5. Moment Analysis

Weighted least squares (WLS) regression was used to estimate the parameters of the drainage area-only power-mean scaling relation equation (7) for several moment orders (Table 2). We considered power averages with positive and negative moment orders that range in magnitude from $|r| = 0.1$ through to $|r| = 5$ at a step of 0.1 and from $|r| = 5$ to $|r| = 10$ at an interval of 1. The geometric mean was used to compute the power average when $r = 0$. Observations were weighted by observed record length. The high values of R^2, all above 0.84, suggest a strong linear relationship between the r^{th} power average and drainage area for all positive integer moment orders. The R^2 increases and the variability of residuals decreases as the moment

Table 1. Summary of Basin Characteristics Considered in This Analysis, With Pearson Correlation Between the Logarithms of the Variable and the Drainage Area Noted[a]

Variable Name	Description	Units	Log-Space Correlation	Significance of Correlation
BDAVE	Average bulk density of the soils in the basin.	Grams per cubic centimeter	−0.0206	0.7876
CDL_CORN	Fraction of the watershed covered by corn cropland. (Class 1 of the 2009 USDA NASS Cropland Data Layer.)	Percent	**0.1314**	**0.0998**
CDL_SOYBEANS	Fraction of the watershed covered by soybean cropland. (Class 5 of the 2009 USDA NASS Cropland Data Layer.)	Percent	−0.0456	0.5851
CLAYAVE	Average clay content of the soils in the basin.	Percent	**0.2272**	**0.0027**
CONTACT	Index of subsurface flow contact time. The subsurface contact time index estimates the number of days that infiltrated water resides in the saturated subsurface zone of the basin before discharging into the stream.	Days	**0.1735**	**0.0224**
CORNSOYBEAN_index	Total fraction of the watershed covered by corn or soybean cropland.	Percent	**0.1360**	**0.0874**
DEVHINLCD06	Fraction of the watershed covered by high-intensity development. (Class 24 of the 2006 National Landcover Data set.)	Percent	0.0774	0.3873
DEVLOWMEDHI_index	Fraction of the watershed covered by high-, medium-, and low-intensity development. (Sum of classes 22, 23, and 24 of the 2006 National Landcover Data set.)	Percent	**0.3062**	**0.0001**
DEVLOWNLCD06	Fraction of the watershed covered by low-intensity development. (Class 22 of the 2006 National Landcover Data set.)	Percent	**0.2518**	**0.0010**
DEVMEDHI_index	Fraction of the watershed covered by high- and medium-intensity development. (Sum of classes 23 and 24 of the 2006 National Landcover Data set.)	Percent	**0.3190**	**0.0000**
DEVMEDNLCD06	Fraction of the watershed covered by medium-intensity development. (Class 23 of the 2006 National Landcover Data set.)	Percent	**0.3075**	**0.0001**
DEVNLCD06	Fraction of the watershed classified as urban or developed land. (Sum of classes 21, 22, 23 and 24 of the 2006 National Landcover Data set.)	Percent	**0.2402**	**0.0015**
DRAIN_SQKM	Watershed drainage area.	Square kilometer	1.0000	0.0000
ELEV_MAX_M_BASIN	Maximum watershed elevation. (100 m National Elevation Data set)	Meters	0.0866	0.2570
ELEV_MEDIAN_M_BASIN	Median watershed elevation. (100 m National Elevation Data set)	Meters	−0.0404	0.5976
ELEV_MIN_M_BASIN	Minimum watershed elevation. (100 m National Elevation Data set)	Meters	**−0.1429**	**0.0615**
FROST_INDEX	The difference between the Julian days of the first and last frost.	Days	0.0667	0.3829
FST32F	The average of the mean Julian day of the first freeze. (2 km PRISM, 30 year data set.)	Day of year	0.0699	0.3609
KFACT_UP	Average K-factor for the upper-most soil horizon in each soil component. The K-factor is an erodibility factor which quantifies the susceptibility of soil particles to detachment and movement by water. The K-factor is used in the Universal Soil Loss Equation (USLE) to estimate soil loss by water. Higher values of K-factor indicate greater potential for erosion.	Unitless	0.0138	0.8566
LSTF32	The average of the mean Julian day of the last freeze. (2 km PRISM, 30 year data set.)	Day of year	−0.0517	0.4995
OMAVE	Average organic content of the soils in the basin.	Percent	0.0782	0.3066
PASTURENLCD06	Fraction of the watershed covered by pastures or hay land. (Class 81 of the 2006 National Landcover Data set.)	Percent	**0.2586**	**0.0007**
PERMAVE	Average permeability of the soils in the basin.	Inches/h	−0.0546	0.4757
PET	Mean annual potential evapotranspiration (PET), estimated using the *Hamon* [1961] equation.	mm/yr	0.0723	0.3448
PLANTNLCD06	Fraction of the watershed covered by agricultural land. (Sum of classes 81 and 82 of the 2006 National Landcover Data set.)	Percent	**0.2396**	**0.0018**
PPT_INDEX	Difference between March and October precipitation as a fraction of the average basin precipitation.	Unitless	0.0516	0.4999
PPTAVG_BASIN	Mean annual precipitation for the watershed. (800m PRISM data, 30 year data set.)	centimeter	**−0.3050**	**0.0000**
RFACT	Rainfall and Runoff factor ("R factor" of Universal Soil Loss Equation); average annual value for period 1971–2000.	100s ft-ton in/h/ac/yr	**−0.1316**	**0.0844**
RH_BASIN	Average relative humidity across the basin. (2km PRISM, 30-year data set.)	Percent	−0.0164	0.8307
ROCKDEPAVE	Average thickness of soil samples examined in the basin.	Inches	−-0.0549	0.4731
RRMEDIAN	Dimensionless elevation-relief ratio, calculated as (ELEV_MEDIAN - ELEV_MIN)/(ELEV_MAX - ELEV_MIN).	Unitless	**−0.2082**	**0.0060**
SANDAVE	Average sand content of the soils in the basin.	Percent	−0.0400	0.6009
SILTAVE	Average silt content of the soils in the basin.	Percent	−0.0288	0.7066
SLOPE_PCT	Mean watershed slope, percent. (100 m National Elevation Data set)	Percent	−0.1126	0.1401
T_AVE_BASIN	Average annual air temperature for the watershed. (2 km PRISM, 30 year data set.)	Kelvin (originally degrees C)	0.0657	0.3905
T_INDEX	Difference between the average annual temperature and the difference between the January and July temperatures.	Kelvin (originally degrees C)	−0.0995	0.2372
T_MAX_BASIN	Average of maximum monthly air temperature in the watershed. (800 m PRISM data, 30 year data set.)	Kelvin (originally degrees C)	0.0913	0.2322
TEMP_MIN	Average of minimum monthly air temperature in the watershed. (800 m PRISM data, 30 year data set.)	Kelvin (originally degrees C)	0.0602	0.4318
TOPWET	Topographic wetness index, ln(a/S); where "ln" is the natural log, "a" is the upslope area per unit contour length and "S" is the slope at that point. See http://ks.water.usgs.gov/Kansas/pubs/reports/wrir.99–4242.html and *Wolock and McCabe* [1995] for more detail.	ln(m)	**0.1901**	**0.0122**

Table 1. (continued)

Variable Name	Description	Units	Log-Space Correlation	Significance of Correlation
WATERNLCD06	Fraction of the watershed covered by open water. (Class 11 of the 2006 National Landcover Data set.)	Percent	**0.3192**	**0.0000**
WOODYWETNLCD06	Fraction of the watershed covered by woody wetlands. (Class 90 of the 2006 National Landcover Data set.)	Percent	0.0956	0.2151
WTDEPAVE	Average depth to the seasonally high water table in the watershed.	Feet	−0.0993	0.1937

[a]Bolded correlations are significant at the 10% level.

order increases from $r = -10$ to $r = 2$, increasing most rapidly between $r = -2$ and $r = 2$. The goodness-of-fit peaks around the first and second moments. The low R^2 values associated with the lower flows indicate that drainage area alone was unable to capture the behavior of low flows.

Because equation (7) estimates the scaling exponent β_r directly, it can be graphed with confidence intervals against the moment orders and its behavior observed directly. This result is shown in Figure 2; this curve represents the moment scaling function or signature of the region from the analysis of drainage area alone. The scaling exponent has a maximum at a moment order of $r = 1$ (the mean flow), with $\beta_1 = 0.915 \pm 0.035$. The exponents decrease moving away from the mean until, at the extremes the moments scale similarly, with mean exponents between 0.8 and 0.75, though the exponents associated with large magnitude negative moment orders have a larger uncertainty.

For high flows, moving away from the mean, the declines in scaling exponents indicate decreasing variability (i.e., a thinner-tailed distribution) with increasing scale. This agrees with most results for the scaling of flood flows [*Gupta et al*., 1994]. For low flow, the decline moving away from the mean indicates increasing variability (i.e., a fatter-tailed distribution) with scale. This result is counterintuitive: it would suggest base flow recessions, for example, are more extended for small basins than for large ones. At the same time, these decreasing exponents suggest that the effective contributing drainage area ($A^{\beta r}$) shrinks as the moment order departs from one, suggesting, in this case, that a smaller fraction of the drainage area contributes to both high and low flows as compared to mean flows. Another interpretable property of such curves is the scaling of the arithmetic mean ($r = 1$), which is an indicator of mass conservation. As noted, for this drainage area-only analysis, this exponent is 0.915 ± 0.035, indicating a systematic decrease of flow per unit area as drainage area increases. Such a result is not hydrologically impossible, but it is surprising for a humid region [*Glymph and Holtan*, 1969, Figure 19; *Wolman and Gerson*, 1978, Figure 1].

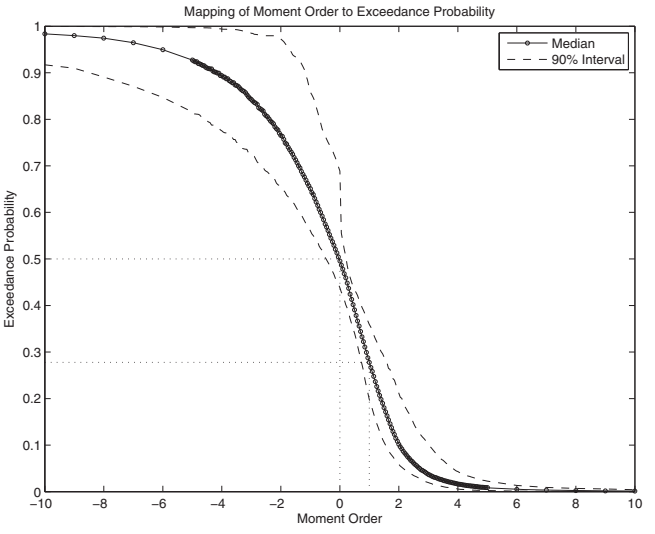

Figure 1. Mapping of moment orders to exceedance probabilities by equating power means and quantiles for moment orders between −10 and 10. The 90% interval shown ranges from the 5th to the 95th percentile across sites at each moment order.

In light of these apparently anomalous results from the drainage area-only analysis, an investigation of the possible effect of OVB on the drainage area scaling is indicated. As discussed, neglecting variables that are both significant to the model and significantly correlated with drainage area can affect the estimate of the spatial scaling exponent. Physically, as the drainage area is not the only characteristic driving flow, it seems inherently flawed to consider its explanatory power in isolation. For this reason, additional explanatory variables should be brought into the model in order to more accurately represent the scaling exponent and address OVB.

Table 2. Summary of Regression Results for Integer Moment Orders When Drainage Area (DRAIN_SQKM) Is the Only Explanatory Variable

Moment Order	Intercept	T-Stat (Intercept)	Scaling Exponent	T-Stat (Scaling Exponent)	Residual SD	R2
−10	−2.5824	−3.8654	0.7750	8.4892	1.6129	0.2788
−9	−2.5398	−3.8289	0.7786	8.5890	1.6012	0.2835
−8	−2.4917	−3.7935	0.7831	8.7240	1.5855	0.2897
−7	−2.4373	−3.7625	0.7890	8.9121	1.5638	0.2984
−6	−2.3749	−3.7408	0.7967	9.1834	1.5330	0.3106
−5	−2.3014	−3.7365	0.8072	9.5899	1.4883	0.3286
−4	−2.2136	−3.7659	0.8217	10.2292	1.4215	0.3566
−3	−2.1032	−3.8556	0.8414	11.2873	1.3193	0.4022
−2	−1.9207	−4.0202	0.8614	13.1928	1.1535	0.4810
−1	−1.6070	−4.3279	0.8762	17.2673	0.8856	0.6239
0	−1.2287	−5.3807	0.8980	28.7756	0.5286	0.8332
1	−0.7564	−5.7663	0.9146	51.0246	0.3089	0.9389
2	0.0608	0.5232	0.8874	55.8872	0.2896	0.9441
3	0.9665	7.0118	0.8430	44.7574	0.3447	0.9155
4	1.6195	10.3670	0.8164	38.2426	0.3889	0.8893
5	2.0505	12.2147	0.8037	35.0343	0.4169	0.8718
6	2.3446	13.3672	0.7978	33.2833	0.4351	0.8604
7	2.5555	14.1571	0.7950	32.2278	0.4476	0.8526
8	2.7139	14.7381	0.7937	31.5418	0.4566	0.8472
9	2.8372	15.1879	0.7932	31.0695	0.4634	0.8432
10	2.9361	15.5493	0.7929	30.7294	0.4686	0.8401

In order to assess the impacts of OVB, the variables in Table 1 were incorporated into the scaling analysis to estimate the multivariate power average regression model (equation (12)) for each moment order. For reference, the correlations between the drainage area and each explanatory variable are included in the table, with the significant ($\alpha = 10\%$) correlations indicated. Variable selection for these regressions was carried out by stepwise regression. The resulting models are summarized in Table 3 for the integer moment orders. The adjusted R^2 of these models is greater than the R^2 for the drainage area-only models. The increase is most dramatic for negative moment orders, reinforcing the conclusion that drainage area alone did not capture the behavior of the inverse moments. In addition, this shows that additional variables can significantly increase the explanatory power of the regressions. Among the integer-order moments in Table 3, the adjusted R^2 peaks at the arithmetic mean ($r = 1$), which is near where the scaling exponent crosses one. (Numerous variables were included in each regression. Because the sample size is large, the true model is unknown and interest lies only in the unbiased estimate of the scaling exponent, the results of *Kroll and Song* [2013] suggest that multicollinearity should not be a primary concern.)

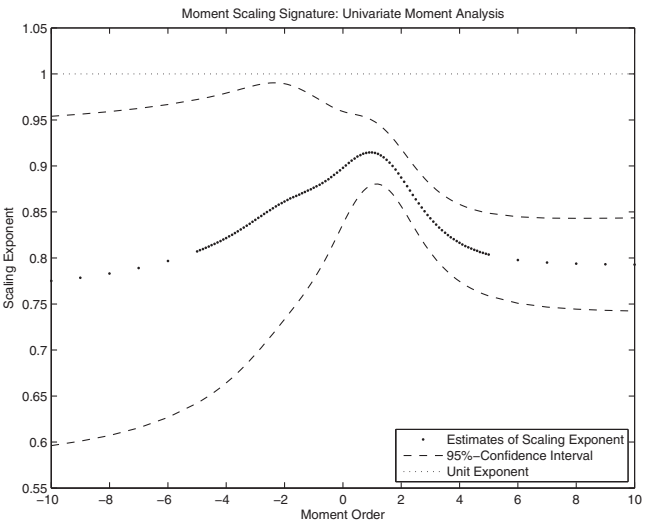

Figure 2. Moment scaling signature for univariate moment analysis relying on drainage area (DRAIN_SQKM) alone.

The moment scaling signature in Figure 3 shows a different picture than was seen before in the drainage-area only results. Previously, all scaling exponents were less than one; here the scaling exponent is broadly monotonically decreasing and crosses from greater than to less than one between moment orders $r = 0.5$ and $r = 1.1$, where the adjusted R^2 peaks. (Local fluctuations in the scaling exponent arise at least in part from changes in the selected explanatory variables in the regressions, which are done independently among moment orders.) The scaling exponent

Table 3. Summary of Regression Results for Integer Moment Orders When Regression Is Applied With Consideration of All Variables Available[a]

Moment Order	Scaling Exponent	Max VIF	Residual SD	AdjR2	Number of Coefficients (Including Intercept)	Variables
−10	1.1064	16.7119	1.0542	0.6704	14	Intercept, **PPTAVG_BASIN**, SLOPE_PCT, OMAVE, ROCKDEPAVE, WTDEPAVE, BDAVE, **RFACT**, TEMP_MIN, **WATERNLCD06**, **PASTURENLCD06**, T_INDEX, DEVHINLCD06
−9	1.1080	16.7119	1.0435	0.6746	14	Intercept, **PPTAVG_BASIN**, SLOPE_PCT, OMAVE, ROCKDEPAVE, WTDEPAVE, BDAVE, **RFACT**, TEMP_MIN, **WATERNLCD06**, **PASTURENLCD06**, T_INDEX, DEVHINLCD06
−8	1.1097	16.7119	1.0296	0.6800	14	Intercept, **PPTAVG_BASIN**, SLOPE_PCT, OMAVE, ROCKDEPAVE, WTDEPAVE, BDAVE, **RFACT**, TEMP_MIN, **WATERNLCD06**, **PASTURENLCD06**, T_INDEX, DEVHINLCD06
−7	1.1117	16.7119	1.0110	0.6869	14	Intercept, **PPTAVG_BASIN**, SLOPE_PCT, OMAVE, ROCKDEPAVE, WTDEPAVE, BDAVE, **RFACT**, TEMP_MIN, **WATERNLCD06**, **PASTURENLCD06**, T_INDEX, DEVHINLCD06
−6	1.1537	42.7104	0.9768	0.7014	14	Intercept, **PPTAVG_BASIN**, SLOPE_PCT, SILTAVE, OMAVE, ROCKDEPAVE, WTDEPAVE, BDAVE, TEMP_MIN, **WATERNLCD06**, **PASTURENLCD06**, PET, DEVHINLCD06
−5	1.1553	42.7104	0.9408	0.7141	14	Intercept, **PPTAVG_BASIN**, SLOPE_PCT, SILTAVE, OMAVE, ROCKDEPAVE, WTDEPAVE, BDAVE, TEMP_MIN, **WATERNLCD06**, **PASTURENLCD06**, PET, DEVHINLCD06
−4	1.1634	6.2652	0.9140	0.7222	11	**PPTAVG_BASIN**, SLOPE_PCT, SILTAVE, OMAVE, ROCKDEPAVE, WTDEPAVE, BDAVE, **WATERNLCD06**, **PASTURENLCD06**, DEVHINLCD06
−3	1.1432	6.1984	0.8284	0.7528	12	Intercept, **PPTAVG_BASIN**, SLOPE_PCT, SILTAVE, OMAVE, ROCKDEPAVE, WTDEPAVE, BDAVE, **WATERNLCD06**, **PASTURENLCD06**, DEVHINLCD06
−2	1.1277	2.8709	0.7249	0.7879	10	Intercept, **PPTAVG_BASIN**, SLOPE_PCT, SILTAVE, OMAVE, ROCKDEPAVE, **PLANTNLCD06**, **WATERNLCD06**, DEVHINLCD06
−1	1.0951	3.8736	0.4976	0.8759	12	Intercept, **PPTAVG_BASIN**, SLOPE_PCT, **CLAYAVE**, SILTAVE, OMAVE, ROCKDEPAVE, **WATERNLCD06**, **PASTURENLCD06**, **RRMEDIAN**, DEVHINLCD06
0	1.0304	4.9873	0.2485	0.9620	11	Intercept, **PPTAVG_BASIN**, SLOPE_PCT, ELEV_MAX_M, **CLAYAVE**, SILTAVE, OMAVE, ROCKDEPAVE, **PASTURENLCD06**, DEVHINLCD06
1	0.9956	16.7398	0.1206	0.9906	8	Intercept, **PPTAVG_BASIN**, SILTAVE, WTDEPAVE, T_MAX_BASIN, T_INDEX, DEVHINLCD06
2	0.9335	48.7036	0.1754	0.9784	10	Intercept, **PPTAVG_BASIN**, ELEV_MAX_M, SILTAVE, ROCKDEPAVE, **RFACT**, TEMP_MIN, PET, T_INDEX
3	0.8562	5.7430	0.2457	0.9547	10	Intercept, ELEV_MAX_M, **CLAYAVE**, OMAVE, ROCKDEPAVE, **RFACT**, **PLANTNLCD06**, CDL_SOYBEA, T_INDEX
4	0.8821	9.5494	0.3007	0.9304	10	Intercept, **PPTAVG_BASIN**, ELEV_MAX_M, ELEV_MIN_M, SILTAVE, ROCKDEPAVE, RH_BASIN, **PLANTNLCD06**, CDL_SOYBEAN
5	0.8259	1.7764	0.3504	0.9066	6	Intercept, SILTAVE, ROCKDEPAVE, **RFACT**, CDL_SOYBEAN
6	0.8200	1.7764	0.3721	0.8947	6	Intercept, SILTAVE, ROCKDEPAVE, **RFACT**, CDL_SOYBEAN
7	0.8171	1.7764	0.3870	0.8864	6	Intercept, SILTAVE, ROCKDEPAVE, **RFACT**, CDL_SOYBEAN
8	0.8157	1.7764	0.3978	0.8804	6	Intercept, SILTAVE, ROCKDEPAVE, **RFACT**, CDL_SOYBEAN
9	0.8150	1.7764	0.4058	0.8759	6	Intercept, SILTAVE, ROCKDEPAVE, **RFACT**, CDL_SOYBEAN
10	0.8147	1.7764	0.4119	0.8725	6	Intercept, SILTAVE, ROCKDEPAVE, **RFACT**, CDL_SOYBEAN

[a]Variables that showed a significant correlation with drainage area are included in bold.

for the arithmetic mean is $\beta_1 = 0.996 \pm 0.013$, which encompasses a unit exponent. As the unit exponent for the arithmetic mean indicates conservation of mass, this result is more intuitive in this humid area than the drainage-area-only estimate of the scaling exponent of the mean, which was less than one. The broadly monotonically decreasing scaling exponent shows that variability decreases with scale for high and low flows and the effective contributing drainage area ratio decreases, relative to its nominal value. In this way, accounting for OVB significantly alters the estimate and interpretation of the scaling exponent.

The effects of OVB can be more readily seen by comparing the separate moment scaling signatures on the same axes, as shown in Figure 4. The horizontal line indicates what simple scaling would look like under the assumption of mass conservation. With just drainage area, the scaling is arguably "simpler" in that the scaling exponent is roughly symmetric around $r = 1$, and moments with orders equally far away from one demonstrate similar scaling exponents. When additional variables are considered, lower-order moments scale in a markedly different fashion than the high moments. Most obviously, the β_r estimates for negative moment orders are greater than one rather than less, and the overall tendency is for β_r to decrease with r, with $\beta_1 \approx 1$ indicating mass conservation, as discussed previously.

In addition to the scaling exponent values, there are a couple of other ways in which negative moments differ from the positive moments once additional variables are included. First, different sets of variables are

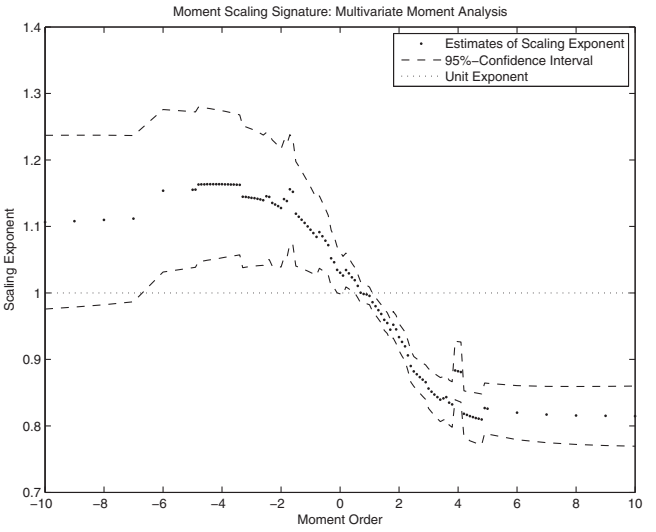

Figure 3. Moment scaling signature for multivariate moment analysis relying on multiple regressions considering all available variables.

significant in explaining the inverse and positive moments. The slope of the basin (SLOPE_PCT) (positive coefficients), organic content of the soil (OMAVE) (negative coefficients), depth to the water table (WTDEPAVE) (negative coefficients), percent of open water (WATERNLCD06) (positive coefficients), extent of pasture land (PASTURENLCD06) (negative coefficients), and the amount of high-density development (DEVHINLCD06) (negative coefficients) commonly play a role in predicting the inverse moments. Positive-order moments are driven significantly by the extent of soybean crops (CDL_SOYBEAN) (negative coefficients). Most moments were affected by the depth to rock in the soil (ROCKDEPAVE) (positive coefficients for negative-order moments, negative coefficients for positive-order moments) and the silt content of the soils (SILT_AVE) (negative coefficients for negative-order moments, positive coefficients for positive-order moments). Basin precipitation (PPTAVG_BASIN) appears in the equations for inverse and small positive order moments with large positive coefficients, which decrease as the moment orders increase. The R (rainfall erosivity) factor of the Universal Soil Loss Equation (RFACT), a precipitation measure that is sensitive to intense precipitation [*D'Odorico et al*., 2001; *Hollinger et al*., 2002], appears in both negative and positive order moments but is more common and more significant in high positive order moment equations; RFACT appears in those equations with a positive coefficient when PPTAVG_BASIN disappears.

These results indicate some physically reasonable relationships: SLOPE_PCT, with its positive coefficients for negative-order moments, indicates the importance of gravity in maintaining streamflow during relatively low-water periods. Similarly, ROCKDEPAVE, an indicator of soil depth, with its positive coefficients for negative-order moments and negative coefficients for positive-order moments, shows that deep soils tend to increase streamflow during low-water periods but reduce it during high-water periods. The switch in precipitation variables from PPTAVG_BASIN to RFACT, the latter being more indicative of precipitation intensity, at high positive-order moments also makes physical sense.

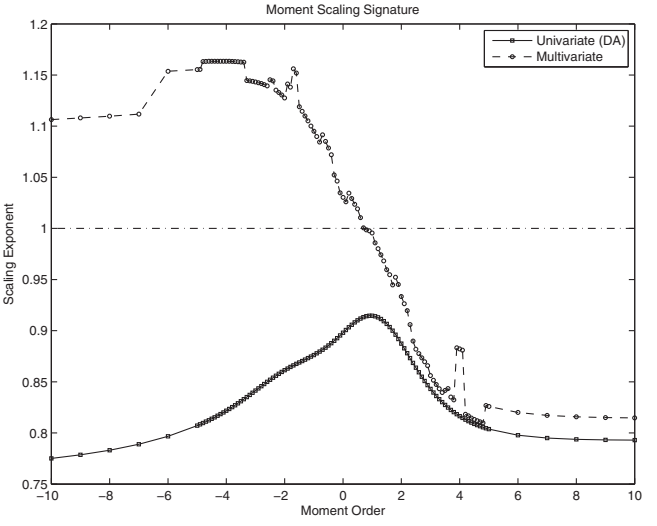

Figure 4. Moment scaling signatures for univariate and multivariate moment analysis.

In addition to the differences in explanatory variables, all methods showed that the regression relationships were weaker for the inverse moments, as indicated by their substantially lower adjusted R^2 values. This shows that the explanatory variables available in this study only partially captured the behavior of low flows. Possible causes of this phenomenon are considered in the Discussion section below.

6. Quantile Analysis

Moment scaling analysis can be somewhat inaccessible because it is difficult to interpret the physical

Table 4. Summary of Regression Results for Quantile Analysis With Drainage Area (DRAIN_SQKM) as the Only Explanatory Variable

Exceedance Probability	Intercept	T−Stat (Intercept)	Scaling Exponent	T−Stat (Scaling Exponent)	Residual SD	R2
0.0005	3.0091	19.3737	0.8179	38.5350	0.3905	0.8900
0.0050	1.7342	12.2964	0.8808	45.6995	0.3515	0.9193
0.0100	1.2666	9.6003	0.9026	50.0613	0.3289	0.9317
0.0250	0.6096	5.0250	0.9302	56.1116	0.2979	0.9461
0.0500	0.1334	1.1437	0.9441	59.2420	0.2825	0.9524
0.1000	−0.2914	−2.4057	0.9475	57.2429	0.2924	0.9490
0.1500	−0.4937	−3.8310	0.9409	53.4285	0.3095	0.9421
0.2000	−0.6404	−4.6124	0.9346	49.2561	0.3306	0.9335
0.2500	−0.7564	−5.0631	0.9282	45.4650	0.3527	0.9238
0.3000	−0.8528	−5.2837	0.9211	41.7615	0.3778	0.9123
0.4000	−1.0224	−5.4028	0.9063	35.0493	0.4366	0.8827
0.5000	−1.2156	−5.4320	0.8948	29.2583	0.5143	0.8408
0.6000	−1.4175	−5.2968	0.8823	24.1268	0.6130	0.7823
0.7000	−1.6480	−5.2322	0.8730	20.2819	0.7275	0.7116
0.7500	−1.7782	−5.2511	0.8699	18.7972	0.7866	0.6760
0.8000	−1.9167	−5.2715	0.8668	17.4451	0.8491	0.6388
0.8500	−2.0890	−5.3681	0.8661	16.2862	0.9132	0.6032
0.9000	−2.2914	−5.4842	0.8653	15.1544	0.9853	0.5643
0.9500	−2.5622	−5.5964	0.8630	13.7935	1.0897	0.5117
0.9750	−2.7722	−5.6569	0.8594	12.8331	1.1773	0.4701
0.9900	−2.9811	−5.6357	0.8520	11.7861	1.2791	0.4226
0.9950	−3.1230	−5.6030	0.8473	11.1237	1.3517	0.3932
0.9995	−3.2286	−4.9728	0.7988	9.0032	1.5751	0.2996

meaning of moment orders other than $r = 1$ (the mean). For this reason, quantile scaling is an attractive alternative method to evaluate the behavior of the spatial scaling exponent β_p. Again, because all quantiles are in units of streamflow, the regression slope estimate of the linearized form of *Eq*. (11) at each exceedance probability provides a direct, though approximate, estimate of β_p. Furthermore, quantile analysis is directly linked to the flow-duration curve, making the relation between scaling factors and flow regimes much more intuitive for interpretation and useful in applications [*Vogel and Fennessey*, 1995]. As will be shown, quantile and moment analysis often, though not always, lead to similar conclusions.

We first applied quantile analysis with WLS regression on drainage area alone; results are summarized in Table 4. The regressions have high goodness-of-fit for exceedance probabilities less than 0.4 ($R^2 > 0.88$), but drop quickly for low flows (higher exceedance probabilities). As in the moment analysis, here drainage area alone explains the variability of high flows well, but is less explanatory for low flows. As can be seen more clearly in the quantile scaling signature of Figure 5, the scaling exponent is not constant across the flow duration curve, leading to the conclusion that flows in this region do not exhibit simple scaling. The spatial scaling exponent is greatest for moderately high flows (near an exceedance probability of 0.1) and reduces rapidly for both extreme high and low flows; the decline is much more gradual toward higher exceedance probabilities (lower flows). This finding indicates that the effective contributing drainage area

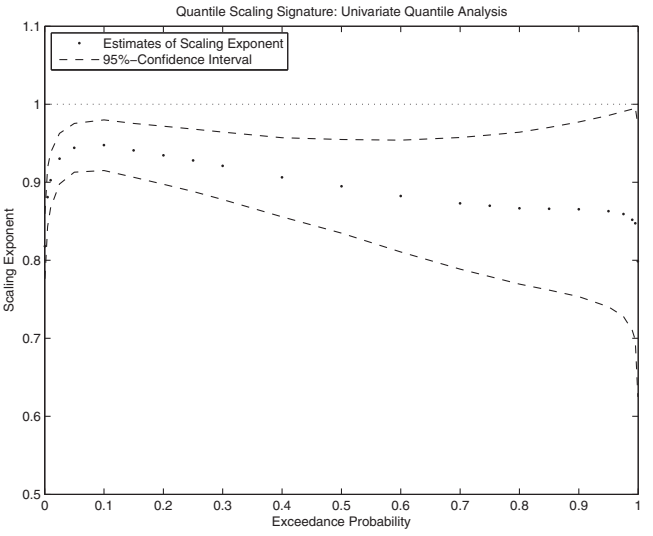

Figure 5. Quantile scaling signature for univariate quantile analysis relying on drainage area (DRAIN_SQKM) alone. The 95% confidence interval is included.

Table 5. Summary of Regression Results for Quantile Analysis When Regression Is Applied With Consideration of All Variables Available[a]

Exceedance Probability	Drainage Area	Max VIF	Residual SD	AdjR2	Number of Coefficients (Including Intercept)	Variables
0.0005	0.8436	9.8127	0.2957	0.9338	9	Intercept, ELEV_MAX_M, SILTAVE, ROCKDEPAVE, **RFACT**, **PLANTNLCD06**, CDL_SOYBEAN, T_INDEX
0.0050	0.8988	9.1620	0.2184	0.9675	8	**CLAYAVE**, OMAVE, ROCKDEPAVE, **RFACT**, TEMP_MIN, WOODYWETNLCD06, T_INDEX
0.0100	0.9273	16.2598	0.1985	0.9739	9	Intercept, SILTAVE, OMAVE, ROCKDEPAVE, **RFACT**, TEMP_MIN, WOODYWETNLCD06, T_INDEX
0.0250	0.9608	11.9238	0.1708	0.9814	10	Intercept, **PPTAVG_BASIN**, ELEV_MAX_M, **CLAYAVE**, OMAVE, ROCKDEPAVE, **RFACT**, TEMP_MIN, T_INDEX
0.0500	0.9895	11.1788	0.1441	0.9872	9	Intercept, **PPTAVG_BASIN**, OMAVE, ROCKDEPAVE, **RFACT**, TEMP_MIN, WOODYWETNLCD06, T_INDEX
0.1000	1.0048	25.6115	0.1336	0.9891	9	Intercept, **PPTAVG_BASIN**, ELEV_MAX_M, OMAVE, ROCKDEPAVE, FST32F, TEMP_MIN, T_MAX_BASIN
0.1500	1.0167	4.6964	0.1333	0.9891	8	Intercept, **PPTAVG_BASIN**, CLAYAVE, SILTAVE, ROCKDEPAVE, T_MAX_BASIN, PERMAVE
0.2000	1.0209	5.5590	0.1345	0.9889	8	Intercept, **PPTAVG_BASIN**, **TOPWET**, SILTAVE, ROCKDEPAVE, T_INDEX, DEVHINLCD06
0.2500	1.0190	230.1006	0.1384	0.9881	9	Intercept, **PPTAVG_BASIN**, T_AVE_BASIN, **TOPWET**, SILTAVE, WTDEPAVE, PET, DEVHINLCD06
0.3000	1.0133	1.8489	0.1534	0.9855	7	Intercept, **PPTAVG_BASIN**, SILTAVE, WTDEPAVE, PET, DEVHINLCD06
0.4000	1.0310	11.9449	0.1703	0.9814	13	Intercept, **PPTAVG_BASIN**, **TOPWET**, **CLAYAVE**, SILTAVE, OMAVE, WTDEPAVE, TEMP_MIN, **PLANTNLCD06**, **PASTURENLCD06**, ELEV_MEDIAN_M_BASIN, DEVHINLCD06
0.5000	1.0285	12.3730	0.2111	0.9720	13	Intercept, **PPTAVG_BASIN**, SLOPE_PCT, ELEV_MAX_M, **CLAYAVE**, SILTAVE, OMAVE, ROCKDEPAVE, WTDEPAVE, **RFACT**, **PASTURENLCD06**, DEVHINLCD06
0.6000	1.0385	12.9574	0.2776	0.9532	13	Intercept, **PPTAVG_BASIN**, SLOPE_PCT, ELEV_MAX_M, **CLAYAVE**, SILTAVE, OMAVE, ROCKDEPAVE, WTDEPAVE, TEMP_MIN, **PASTURENLCD06**, DEVHINLCD06
0.7000	1.0494	4.9873	0.3676	0.9235	11	Intercept, **PPTAVG_BASIN**, SLOPE_PCT, ELEV_MAX_M, **CLAYAVE**, SILTAVE, OMAVE, ROCKDEPAVE, **PASTURENLCD06**, DEVHINLCD06
0.7500	1.0665	20.0420	0.4041	0.9099	13	Intercept, **PPTAVG_BASIN**, SLOPE_PCT, **CLAYAVE**, SILTAVE, OMAVE, ROCKDEPAVE, **RFACT**, TEMP_MIN, **PASTURENLCD06**, T_INDEX, DEVHINLCD06
0.8000	1.0820	3.6291	0.4692	0.8858	10	Intercept, **PPTAVG_BASIN**, SLOPE_PCT, **CLAYAVE**, SILTAVE, OMAVE, ROCKDEPAVE, **PASTURENLCD06**, DEVHINLCD06
0.8500	1.0873	3.8736	0.5107	0.8698	12	Intercept, **PPTAVG_BASIN**, SLOPE_PCT, **CLAYAVE**, SILTAVE, OMAVE, ROCKDEPAVE, **WATERNLCD06**, **PASTURENLCD06**, **RRMEDIAN**, DEVHINLCD06
0.9000	1.1021	3.8736	0.5651	0.8496	12	Intercept, **PPTAVG_BASIN**, SLOPE_PCT, **CLAYAVE**, SILTAVE, OMAVE, ROCKDEPAVE, **WATERNLCD06**, **PASTURENLCD06**, **RRMEDIAN**, DEVHINLCD06
0.9500	1.1223	3.8736	0.6470	0.8196	12	Intercept, **PPTAVG_BASIN**, SLOPE_PCT, **CLAYAVE**, SILTAVE, OMAVE, ROCKDEPAVE, **WATERNLCD06**, **PASTURENLCD06**, **RRMEDIAN**, DEVHINLCD06
0.9750	1.1233	2.8034	0.7241	0.7925	10	**PPTAVG_BASIN**, SLOPE_PCT, SILTAVE, OMAVE, ROCKDEPAVE, **WATERNLCD06**, **PASTURENLCD06**, **RRMEDIAN**, DEVHINLCD06
0.9900	1.1461	2.8709	0.8188	0.7552	10	Intercept, **PPTAVG_BASIN**, SLOPE_PCT, SILTAVE, OMAVE, ROCKDEPAVE, **PLANTNLCD06**, **WATERNLCD06**, DEVHINLCD06
0.9950	1.1769	10.7891	0.8593	0.7433	12	Intercept, **PPTAVG_BASIN**, SLOPE_PCT, SILTAVE, OMAVE, ROCKDEPAVE, TEMP_MIN, **PLANTNLCD06**, **WATERNLCD06**, ELEV_MEDIAN_M_BASIN, DEVHINLCD06
0.9995	1.1311	2.8152	1.0829	0.6582	9	**PPTAVG_BASIN**, SLOPE_PCT, SILTAVE, ROCKDEPAVE, BDAVE, **WATERNLCD06**, **PASTURENLCD06**, DEVHINLCD06

[a]Variables that showed a significant correlation with drainage area are included in bold.

ratio decreases toward the tails of the distribution. Agreeing with most results on flood flows [*Gupta et al.*, 1994], high flows have decreasing variability with scale, while the variability of low flows increases with scale. Further, the maximum scaling exponent is less than one throughout, suggesting that there is no quantile where mass conservation holds, another surprising (or anomalous) result.

As in the moment analysis with drainage area alone, these surprising interpretations lead to the suspicion that OVB is occurring. The impact of OVB was again assessed by applying a multiple-regression framework that allows for the impacts of additional variables, especially those correlated with drainage area. These results are displayed in Table 5, and the resultant quantile scaling signature is shown in Figure 6. Including the additional variables produced a marked improvement in adjusted R^2, indicating a better model and therefore a better estimate of the scaling exponent at each quantile. As with the moment scaling analysis, the improvements are most dramatic in the low flows (high exceedance probabilities), showing that omitted variables are most needed in predicting low flows. The importance of the omitted variables at low flows is reinforced in the quantile scaling signature, where the scaling exponent at an exceedance probability of 0.1, which had the maximum exponent for the drainage-area only results, is now near one and the decline toward low flows has become a steady increase with a sharp upward tail. This change in low-flow scaling

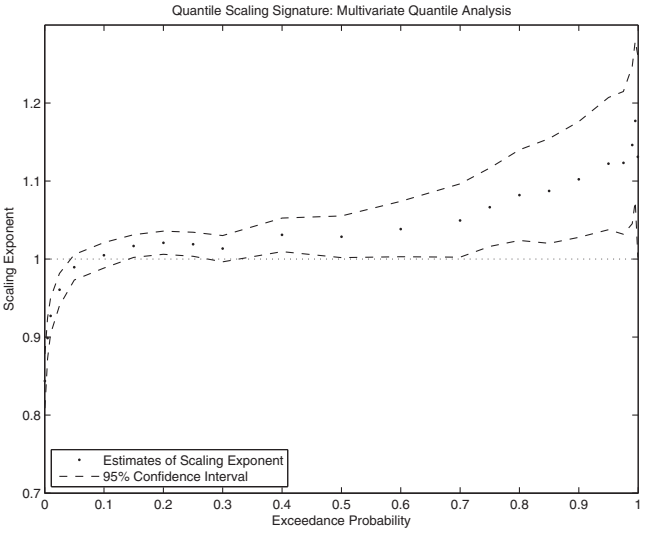

Figure 6. Quantile scaling signature for multivariate quantile analysis relying on multiple regressions considering all available variables.

indicates that there are variables other than drainage area that are affecting the generation of low flows particularly. This finding shows that the nonconservation of mass and apparent increasing variability with scale that appeared in the drainage area-only quantile analysis resulted from the failure to account for these other variables.

Examination of the explanatory variables used in the multiple regressions for the quantile scaling analysis (Table 5) shows similar results as appear in Table 3 for the multiple regressions for the moment scaling analysis. For example, PPTAVG_BASIN (again having positive coefficients) is used except at the extreme high flow end, where RFACT appears to substitute for it. Similarly SLOPE_PCT (again with positive coefficients) appears in the lower flow half of the equations. ROCKDPEAVE appears for most low-flow equations, and its coefficients switch from positive to negative when moving from low to high flows. PASTURENLCD06 and DEVHINLCD06 both appear with negative coefficients in most of the lower flow equations.

The two quantile scaling signatures derived are redisplayed in Figure 7. This presentation further highlights the effect of OVB on the interpretation of scaling. A multiple-regression framework provides a different view of the scaling relationship. This difference is most apparent in the scaling exponents associated with low flows (high exceedance probabilities). When regressing against drainage area alone, the scaling signature is smoother. Occurring at an exceedance probability near 0.1, the maximum exponent is 0.95. From this peak, the exponent steeply declines for high and low extremes. The signature from the multiple regressions shares the steep decline at the extreme high flow but then crosses a value of one at an exceedance probability of about 0.1 and rises slowly across the moderate and low flows to a maximum of about 1.15. From this figure, mitigating the effect of OVB results in a more interpretable (and possibly less anomalous) scaling relationship.

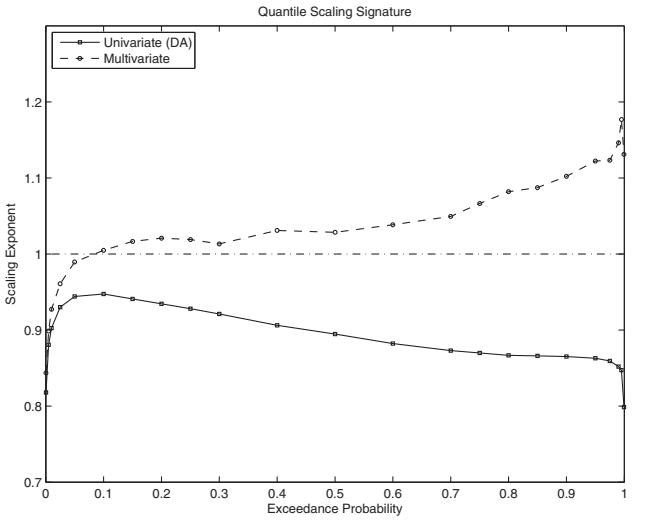

Figure 7. Quantile scaling signatures for univariate and multivariate quantile analysis.

7. Discussion

The conclusions pertaining to scaling behavior based on moment and quantile analysis can be compared with the use of the median of the power mean-based mapping of moment orders to exceedance probabilities presented above (Figure 1). The scaling signatures resulting from the regressions making use of all available variables are shown in Figure 8 (top); the Figure 8 (bottom) shows the corresponding adjusted R^2 values.

Despite being derived from different modes of analysis, these

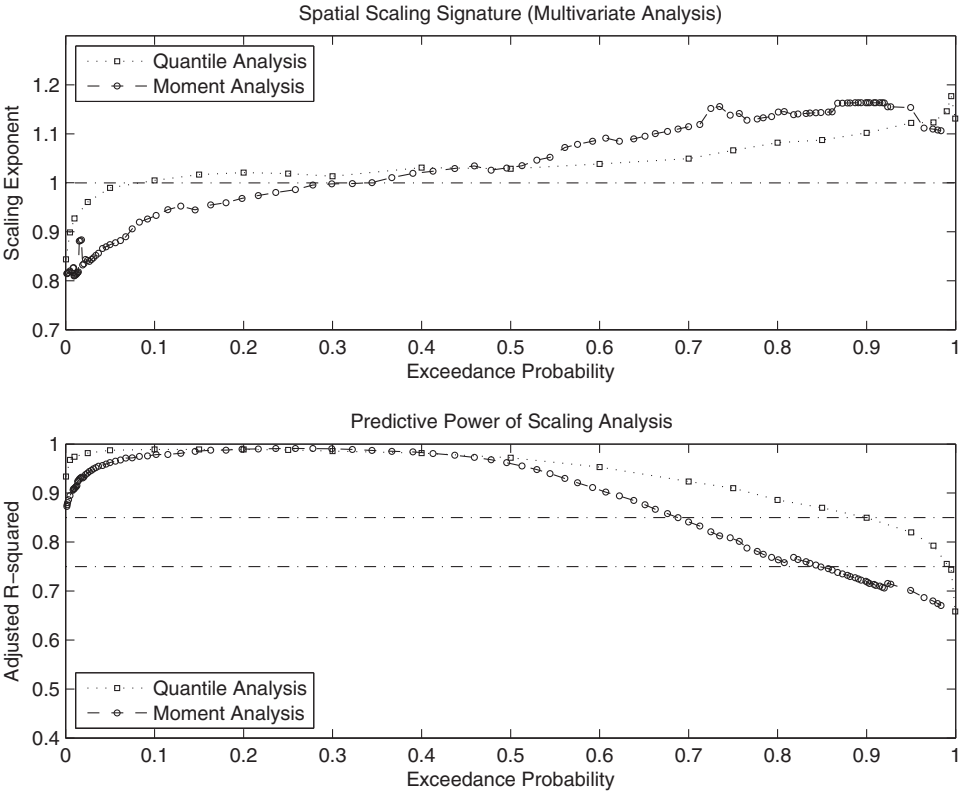

Figure 8. (top) Spatial scaling signatures derived from multivariate moment and quantile analyses. (bottom) Adjusted R^2 of multivariate moment and quantile analyses across exceedance probabilities.

scaling signatures show broadly similar spatial scaling behavior. Both signatures are marked by three distinct regions along the axis of exceedance probabilities. There is a significant decline in scaling factors for high flows, i.e., flows with exceedance probabilities less than about 15%, though this decline is steeper and occurs at a lower exceedance probability in the quantile-derived signature. Between exceedance probabilities of 15% and 70%, the scaling exponents slope upward as the exceedance probabilities increase (i.e., as flows get lower). In this region, the scaling factors are close to one or just above one. Beyond exceedance probabilities of 70%, the moment-based scaling function levels off while the quantile-based function continues it gentle upward rise. As both spatial scaling signatures broadly increase with exceedance probability and cross a value of one, the expected phenomena of decreasing variability with increasing flows and mass conservation at some exceedance probability near 0.1 for the quantile scaling analysis and near the mean (0.28) for the moment scaling analysis are indicated.

Overall, the moment analysis indicates scaling exponents less than those estimated from quantile analysis for flows below the median, and greater than those from quantile analysis for flows above the median, while agreeing at the median and at the low and high extremes (Figure 8, top). The differences in scaling exponents between the two types of analyses appear to indicate deficiencies in the mapping between moment order and exceedance probability. Additionally, it may also be affected by statistical factors such as the sensitivity of high-order moments, whether normal or inverse, to extreme values. The importance of statistical factors in the moment analysis is suggested by the lower adjusted-R^2 values for the moment analysis as compared to the quantile analysis (Figure 8, bottom).

The same general scaling signature that was identified here in the multiple regression results can also be seen in the quantile-based results of *Over et al*. [2014] in Indiana and Illinois—which echo the results of *Singh* [1971] in Illinois—though they take a different approach to the problem of heterogeneity of basin characteristics. A multiple-regression spatial scaling signature for three regions each in Illinois and in Indiana is shown in Figure 9 [see *Over et al*., 2014 for further information]. These results exhibit the same general signature with a midrange plateau, a downturn in the high flows and a gentle upward curvature in the low

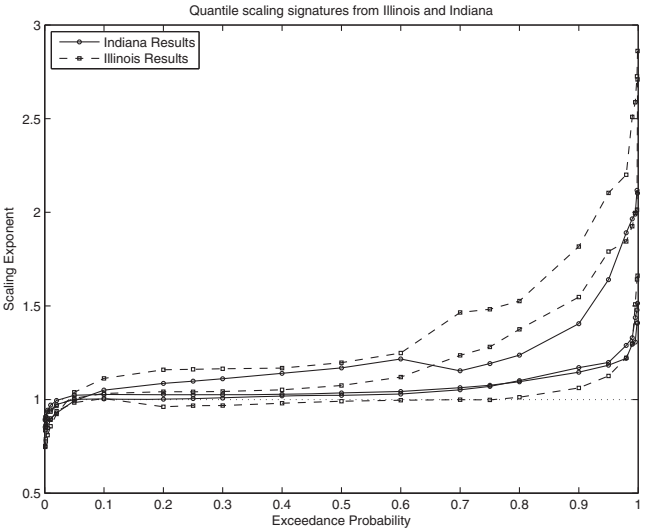

Figure 9. Quantile scaling signatures from multiple regression analysis in Indiana and Illinois [*Over et al*., 2014].

flows. Although the magnitudes of the low-flow scaling factors are much greater, probably because the large number of stations having large numbers of censored (zero) flows are present in the region and were retained in the analysis, the overall signature is quite similar. Interestingly, *Over et al*. [2014] did not find much change in scaling relations resulting from use of multiple regression: they found nearly identical signatures with regressions based on drainage area alone. In their study, the need for multiple regression to get the correct scaling exponent was probably circumvented by classifying the larger region into homogeneous subregions prior to the application of regional regression. This accomplishes the same goal of multiple regression: controlling for regional heterogeneity, especially in basin characteristics that are correlated with both drainage area and the streamflow statistics of interest, in this case.

We hypothesize that the spatial scaling signature exhibited in the study region is a generalizable example of the spatial scaling behavior of streamflow in a given region. As such, the spatial scaling signatures of daily streamflow provide fundamental information as to how streamflow is generated in a specific region. Consider first high flows (floods). When they are rainfall-driven, floods result from the quick response of a basin to extreme storm conditions. The short duration of the flood response and the branching properties of the river network, along with the scale-dependent spatial variability of the precipitation itself [*Gupta and Waymire*, 1993; *Over and Gupta*, 1996], combine to cause a decreasing fraction of the basin to be contributing to the streamflow at a given point and time, as also suggested by the decreasing effective contributing drainage area ratio discussed here. These effects result in a scaling exponent less than one, as shown by the simple model of *Gupta et al*. [1996]. In particular, in both this study region and the results from Indiana and Illinois [*Over et al*., 2014], the high-flow scaling exponent was seen to decrease with decreasing exceedance probability, as has been observed for annual flood peaks in regions including parts of the one considered in this study, with primarily rainfall-generated floods [*Gupta et al*., 1994; *Gupta and Dawdy*, 1995; *Smith*, 1992].

Similar logic can be applied to propose a physical mechanism for the observed scaling properties for low flows. Under conditions when the basin response is changing slowly, low flows result from groundwater outflow. By themselves, such conditions would suggest a scaling exponent of one, since the scale-dependent variability and quick response aspects of high flows have dissipated. However, groundwater flows have their own scale-dependent structure. As originally proposed by *Tóth* [1963] and extended by *Freeze and Witherspoon* [1967], *Ophori and Tóth* [1990], *Cardenas* [2007], and *Wörman et al*. [2007] (see also *Dingman* [2002], chapter 8), the nested structure of a river basin's topography tends to induce a similarly nested set of groundwater flow systems, with important implications for basin response. The discharge from this hierarchy of groundwater flow systems results in increasing fractions of the upstream recharge contributing to base flow as the basin scale gets larger, thus implying a scaling exponent exceeding one, and agreeing with the increased effective contributing drainage area ratio proposed here. In addition, because the larger, deeper systems have longer time scales to depletion, they will increasingly dominate the flow as the exceedance probability increases, causing the scaling exponent to increase with the exceedance probability. Interregional differences in the low-flow scaling were observed: the scaling exponent at extreme low flows in this study region was seen to rise to about 1.2; whereas in Illinois and Indiana, albeit with censored data included, the scaling exponent rose to a value between 1.4 and 3, depending on the subregion [*Over et al*., 2014].

Finally, the midrange of flows on the exceedance probability axis may be characterized as normal or equilibrium conditions. Flows in this region are characterized by scaling factors around one (or slightly above one if there is a significant impact of the hierarchy of groundwater systems on average flows). The assertion of the unit scaling exponent for average flows can be seen by considering a set of streamgages along a single river network with perfectly homogeneous climate, land use, and all basin characteristics. In such a case, the long-term average flow per unit area, in order to conserve mass, should be constant, implying a scaling factor of one.

We suggest that the spatial scaling signatures of daily streamflow constitute a powerful tool for the characterization of streamflow regimes in varied regions. The magnitude and interplay of the three characteristic regions of the spatial scaling signature may provide insight on the behavior of streamflow in a given region, providing insights as to the main drivers of streamflow and allowing recognition of significant changes in the streamflow regime. As has been shown here, multiple regression or another means can be used to isolate these varied effects and reveal a more accurate spatial scaling signature, which in turn provides a better understanding of regional streamflow behavior.

8. Summary and Conclusions

This work has sought to improve our understanding of the spatial scaling behavior of daily streamflow. Scaling behavior has long been interpreted by distinguishing between simple scaling and multiscaling. These notions form the basis of many regional hydrologic methods, including the index-flood method [*Dalrymple*, 1960], regional hydrologic regression [*Tasker and Stedinger*, 1987; *Reis* III, 2007], and the drainage-area ratio transfer method used for prediction in ungaged basins (as in *Farmer and Vogel* [2013]). Assessments of spatial scaling behavior were conducted by examining the relationship between scaling factors and either streamflow moments (moment analysis) or quantiles (quantile analysis). Both analyses estimate scaling exponents using methods of regression. We document a significant deficiency in traditional univariate scaling analysis and advocate a multivariate technique for improving the interpretation of scaling behavior.

Our analyses led to two important sets of findings, one set methodological and another empirical. The methodological findings were twofold. First it was shown that the entire scaling behavior of streamflow moments can be captured only by including inverse moments in the analysis. This was demonstrated by means of an approximate mapping of moment orders to exceedance probabilities, which showed that positive moment orders mapped only to flows above the median, whereas inverse moments mapped to flows below the median. Traditional scaling analysis of flow moments using only positive moments is thus problematic because low flows were demonstrated to scale differently than high flows with respect to drainage area. It was then demonstrated that omitted-variable bias (OVB) can have a significant impact on the assessment of scaling behavior and lead to physically implausible results. OVB resulted from univariate scaling analyses based on drainage area alone. We document that the impact of this bias can be mitigated by the use of multiple regression. When OVB was accounted for with multiple regression, the scaling signatures were distinctly different from those determined using a univariate scaling analysis, and took on forms that were physically plausible and interpretable in terms of the streamflow generating processes for high, midrange, and low flows.

The empirical findings consist of the general form of the OVB-corrected (multiple regression-based) scaling signature in this region. Based on its agreement with results of *Over et al*. [2014] for Illinois and Indiana, we hypothesize that this signature is generally applicable for humid temperate regions. The mean flow was found to scale with a unit exponent, indicating mass conservation. High and low flows were found to have scaling exponents less than and greater than one, respectively. The high flow exponents suggest a decreasing fraction of contributing area with increasing scale and agree with corresponding peak flow analyses, whereas the low-flow exponents suggest an increasing fraction of contributing area with increasing scale. The overall form of the OVB-corrected scaling signature also indicates decreasing variability (thinner tails) of the distribution of flows with increasing scale for both high and low flows.

To our knowledge, no previous analysis of scaling behavior has assessed the impact of OVB nor considered the scaling of inverse streamflow moments. As this study only considered streamflow behavior in the Southeast United States, along with a brief analysis of results from Illinois and Indiana, further research needs to consider the scaling signatures of other regions. Furthermore, future consideration of this topic needs to

examine scaling behavior in a theoretical framework such as that developed by *Gupta et al*. [1996] for floods and seek greater understanding of the physical processes behind these scaling signatures. Special attention needs to be paid to low flows, which, from a scaling perspective, have not received the same degree of attention as high flows. It is our hope that this work and future work will advance our understanding of the characteristics of spatial scaling signatures and how they relate to streamflow-generating processes in a region. Such an understanding will provide advantages for prediction in ungaged basins and the development of water resources in both gaged and ungaged basins.

Appendix A: Effective Contributing Drainage Area Ratio

In interpreting our results, it will be useful to examine equations (6) and (7) more carefully. As defined in equation (4), $E\left[Q_*^r\right]$ designates the r^{th} moment of the streamflow in the unit-area reference watershed. As suggested by previous scaling analyses of peak flow, in particular the toy model of *Gupta et al*. [1996], and also the partial area concept of runoff generation [e.g., *Betson*, 1964; *Dunne and Black*, 1970], it is useful to think of the reference streamflow, Q_*, as consisting of the product of effective contributing drainage area, A_c, and an effective runoff intensity over that contributing area, Q_{eff}, so that $Q_* = A_c Q_{eff}$. According to this model, these quantities, as a product, determine the intercept of our scaling models but cannot be obtained separately by the methods employed in this study.

Then at a basin of drainage area A_i, according to *Eq*. (6), the r^{th} power mean of discharge from that basin

$$\left(E\left[Q_i^r\right]\right)^{1/r} = \left(E\left[\left(A_{c,i}Q_{eff,i}\right)^r\right]\right)^{1/r} \tag{A1}$$

is given by

$$A_i^{\beta_r}\left(E\left[Q_*^r\right]\right)^{1/r} = A_i^{\beta_r}\left(E\left[\left(A_c Q_{eff}\right)^r\right]\right)^{1/r} \tag{A2}$$

That is, the reference basin behavior is simply rescaled by multiplying by $A_i^{\beta_r}$. (Recall that, having been divided by a unit area, A_i is now unitless.) Expanding this expression in terms of the effective contributing drainage area and effective runoff intensity we have

$$\left(E\left[Q_i^r\right]\right)^{1/r} = \left(E\left[\left(A_{c,i}Q_{eff,i}\right)^r\right]\right)^{1/r} = A_i^{\beta_r}\left(E\left[\left(A_c Q_{eff}\right)^r\right]\right)^{1/r} \tag{A3}$$

Similar to the inability to separate the effective contributing drainage area and runoff intensity at the reference basin by using the intercept, how the effective contributing drainage area and runoff intensity separately scale up to drainage area A_i is not available from the analysis presented in this paper.

For purposes of discussion and interpretation, however, assume that the effective runoff intensity is independent of scale, though still depending on moment order, r. In that case, all the rescaling comes from changes in the effective contributing drainage area, A_c, and equation (A3) reduces to

$$\left(E\left[\left(A_{c,i}\right)^r\right]\right)^{1/r} = A_i^{\beta_r}\left(E\left[\left(A_c\right)^r\right]\right)^{1/r} \tag{A4}$$

so that

$$A_i^{\beta_r} = \left(\frac{E\left[\left(A_{c,i}\right)^r\right]}{E\left[\left(A_c\right)^r\right]}\right)^{1/r}. \tag{A5}$$

For simplicity, we can rewrite $\left(E\left[\left(A_{c,i}\right)^r\right]\right)^{1/r}$ as $A_{c,i}(r)$ and $\left(E\left[\left(A_c\right)^r\right]\right)^{1/r}$ as $A_c(r)$. These quantities can be interpreted as the contributing areas of the basin i and the reference basin, respectively, at moment order r. Equation (A5) can then be rewritten as

$$A_i^{\beta_r} = \frac{A_{c,i}(r)}{A_c(r)}. \tag{A6}$$

This expression shows that $A_i^{\beta_r}$ can be interpreted as the ratio of the effective contributing drainage area at the scale of basin i, namely A_i, and moment order r to the effective contributing drainage area of the unit-area reference basin at moment order r. More simply, this term represents the "effective contributing drainage area ratio" at scale A_i and moment order r.

Further, if we divide $A_i^{\beta_r}$ by the total drainage areas A_i, then we have

$$\frac{A_i^{\beta_r}}{A_i} = A_i^{\beta_r - 1} = \frac{A_{c,i}(r)}{A_i A_c(r)}, \tag{A7}$$

This set of equalities shows that $A_i^{\beta_r - 1}$ can be interpreted as the fractional effective contributing area at scale A_i and moment order r. Therefore when the scaling exponent is less than one, the fractional effective contributing area ratio decreases with increasing scale; when the scaling exponent is greater than one, it increases.

An analogous analysis of the quantile representation of the scaling leads to the expression

$$A_i^{\beta_p} = \frac{A_{c,i}(p)}{A_c(p)}, \tag{A8}$$

which can be interpreted as the effective contributing drainage area ratio at scale A_i and exceedance probability p, and to

$$\frac{A_i^{\beta_p}}{A_i} = A_i^{\beta_p - 1} = \frac{A_{c,i}(p)}{A_i A_c(p)}, \tag{A9}$$

The fractional effective contributing drainage area ratio at scale A_i and exceedance probability p.

Note also that when viewed from the perspective of dependence on moment order (r) or exceedance probability (p), this analysis allows for changes in effective contributing drainage area in line with the partial area concept, e.g., as the flows get larger (r gets bigger or p gets smaller), then the effective contributing drainage area A_c and runoff intensity Q_{eff} at the reference scale can also increase. Indeed this increase is given empirically by the intercept terms: $\ln(E[Q_*^r])$ in the case of moment analysis, and $\ln(Q_{*,p})$ in the case of the quantile analysis.

Appendix B: Omitted Variable Bias

Omitted Variable Bias (OVB) is discussed in most textbooks that address multivariate regression in some detail (as in *Wooldridge* [2009]). A brief outline is provided here. The goal of linear regression is to provide estimates of the coefficients in the following relationship:

$$Y = \beta_0 + \beta_1 X_1 + u \tag{B1}$$

where Y is the dependent variable of interest, X is the independent predictor, and u is a normally distributed random error with a mean of zero and a fixed standard deviation. In practice, the slope parameter, β_1, is estimated as

$$\hat{\beta}_1 = \frac{\sum_{i=1}^{n} (X_{1,i} - \bar{X}_1) Y_i}{\sum_{i=1}^{n} (X_{1,i} - \bar{X}_1)^2} \tag{B2}$$

where $\bar{X}$ is the mean value of X, with n paired observations of (X, Y). It can be shown that $\hat{\beta}_1$ is an unbiased estimator of β_1, so that $E[\hat{\beta}_1] = \beta_1$. This is done by plugging equation (B1) into equation (B2), simplifying and taking the expectation, recognizing that the covariance of X and u must be zero.

OVB appears when equation (B1) is not valid. Instead, the true relationship may be something like:

$$Y = \beta_0 + \beta_1 X_1 + \beta_2 X_2 + u \tag{B3}$$

where X_2 is an additional independent variable. Taking the expectation of $\hat{\beta}_1$ with this new knowledge uncovers a systematic bias. Combine equation (B3) into equation (B2) and simplify:

$$\tilde{\beta}_1 = \frac{\sum_{i=1}^{n} (X_{1,i} - \bar{X}_1)(\beta_0 + \beta_1 X_{1,i} + \beta_2 X_{2,i} + u_i)}{\sum_{i=1}^{n} (X_{1,i} - \bar{X}_1)^2} \tag{B4}$$

$$\tilde{\beta}_1=\beta_0\frac{\sum_{i=1}^{n}(X_{1,i}-\bar{X}_1)}{\sum_{i=1}^{n}(X_{1,i}-\bar{X}_1)^2}+\beta_1\frac{\sum_{i=1}^{n}(X_{1,i}-\bar{X}_1)(X_{1,i})}{\sum_{i=1}^{n}(X_{1,i}-\bar{X}_1)^2}+\beta_2\frac{\sum_{i=1}^{n}(X_{1,i}-\bar{X}_1)(X_{2,i})}{\sum_{i=1}^{n}(X_{1,i}-\bar{X}_1)^2}+\frac{\sum_{i=1}^{n}(X_{1,i}-\bar{X}_1)(u_i)}{\sum_{i=1}^{n}(X_{1,i}-\bar{X}_1)^2} \quad \text{(B5)}$$

$$\tilde{\beta}_1=\beta_1+\beta_2\frac{\sum_{i=1}^{n}(X_{1,i}-\bar{X}_1)(X_{2,i})}{\sum_{i=1}^{n}(X_{1,i}-\bar{X}_1)^2}+\frac{\sum_{i=1}^{n}(X_{1,i}-\bar{X}_1)(u_i)}{\sum_{i=1}^{n}(X_{1,i}-\bar{X}_1)^2} \quad \text{(B6)}$$

because $\sum_{i=1}^{n}(X_{1,i}-\bar{X}_1)=0$ and $\sum_{i=1}^{n}(X_{1,i}-\bar{X}_1)(X_{1,i})=\sum_{i=1}^{n}(X_{1,i}-\bar{X}_1)^2$. The expectation of equation (B6) is then

$$E\left[\tilde{\beta}_1\right]=\beta_1+\beta_2E\left[\frac{\sum_{i=1}^{n}(X_{1,i}-\bar{X}_1)(X_{2,i})}{\sum_{i=1}^{n}(X_{1,i}-\bar{X}_1)^2}\right]+E\left[\frac{\sum_{i=1}^{n}(X_{1,i}-\bar{X}_1)(u_i)}{\sum_{i=1}^{n}(X_{1,i}-\bar{X}_1)^2}\right] \quad \text{(B7)}$$

$$E\left[\tilde{\beta}_1\right]=\beta_1+\beta_2\frac{Cov(X_1,X_2)}{Var(X_1)}+\frac{Cov(X_1,u)}{Var(X_1)} \quad \text{(B8)}$$

$$E\left[\tilde{\beta}_1\right]=\beta_1+\beta_2\frac{Cov(X_1,X_2)}{Var(X_1)}\neq\beta_1 \quad \text{(B9)}$$

because $Cov(X_1,u)=0$. So by excluding significant variables that show some correlation with the included variables ($Cov(X_1,X_2)\neq 0$), bias given by $\beta_2\frac{Cov(X_1,X_2)}{Var(X_1)}$ is introduced into the estimator.

Acknowledgments
This study was conducted as a part of the USGS National Water Census and also supports the goals of the National Streamflow Information Program.

References

Betson, R. P. (1964), What is watershed runoff?, *J. Geophys. Res.*, *69*(8), 1541–1552, doi:10.1029/JZ069i008p01541.
Buttle, J. M., and M. C. Eimers (2009), Scaling and physiographic controls on streamflow behavior on the Precambrian Shield, south-central Ontario, *J. Hydrol.*, *374*, 360–372, doi:10.1016/j.jhydrol.2009.06.036.
Cardenas, M. B. (2007), Potential contribution of topography-driven regional groundwater flow to fractal stream chemistry: Residence time distribution analysis of Tóth flow, *Geophys. Res. Lett.*, *34*, L05403, doi:10.1029/2006GL029126.
Dalrymple, T. (1960), Flood frequency analysis, *U.S. Geol. Surv. Water Supply Pap. 1543-A*, U.S. Geol. Surv., Reston, Va.
Dawdy, D. R., and V. K. Gupta (1995), Multiscaling and skew separation in regional floods, *Water Resour. Res.*, *31*(11), 2761–2767, doi:10.1029/95WR02078.
Dingman, S. L. (2002), *Physical Hydrology*, 2nd ed., 646 pp., Prentice Hall, Upper Saddle River, N. J.
D'Odorico, P., J. C. Yoo, and T. M. Over (2001), An assessment of ENSO-induced patterns of rainfall erosivity in the southwestern United States, *J. Clim.*, *14*, 4230–4242, doi:10.1175/1520-0442(2001)014<4230:AAOEIP>2.0.CO;2.
Dunne, T., and R. D. Black (1970), Partial area contributions to storm runoff in a small New England watershed, *Water Resour. Res.*, *6*(5), 1296–1311, doi:10.1029/WR006i005p01296.
Eaton, B., M. Church, and D. Ham (2002), Scaling and regionalization of flood flows in British Columbia, Canada, *Hydrol. Processes*, *16*, 6245–3263, doi:10.1002/hyp.1100.
Falcone, J. (2011), GAGES-II: Geospatial attributes of gages for evaluating streamflow, Database, U.S. Geol. Surv., Reston, Va. [Available at http://water.usgs.gov/lookup/getspatial?gagesII_Sept2011.]
Farmer, W. H., and R. M. Vogel (2013), Performance-weighted methods for estimating monthly streamflow at ungauged sites, *J. Hydrol.*, *477*, 240–250, doi:10.1016/j.jhydrol.2012.11.032.
Freeze, R. A., and P. A. Witherspoon (1967), Theoretical analysis of regional groundwater flow: 2. Effect of water-table configuration and subsurface permeability variation, *Water Resour. Res.*, *3*(2), 623–634, doi:10.1029/WR003i002p00623.
Furey, P. R., and V. K. Gupta (2000), Space-time variability of low streamflow in river networks, *Water Resour. Res.*, *36*(9), 2679–2690, doi:10.1029/2000WR900136.
Glaster, J. C. (2007), Natural and anthropogenic influences on the scaling of discharge with drainage area for multiple watersheds, *Geosphere*, *3*(4), 260–271, doi:10.1130/GES00065.S1.
Glymph, L. M., and H. N. Holtan (1969), Land treatment in agricultural watershed hydrology research, in *Effects of Watershed Changes on Streamflow*, edited by W. L. Moore and C. W. Morgan, pp. 43–68, Univ. of Texas Press, Austin.
Gupta, V. K., and D. R. Dawdy (1995), Physical interpretations of regional variations in the scaling exponents of flood quantiles, *Hydrol. Processes*, *9*, 347–361, doi:10.1002/hyp.3360090309.
Gupta, V. K., and E. Waymire (1990), Multiscaling properties of spatial rainfall and river flow distributions, *J. Geophys. Res.*, *95*(D3), 1999–2009, doi:10.1029/JD095iD03p01999.
Gupta, V. K., and E. C. Waymire (1993), A statistical analysis of mesoscale rainfall as a random cascade, *J. Appl. Meteorol.*, *32*, 251–267, doi:10.1175/1520-0450(1993)032%3C0251:ASAOMR%3E2.0.CO;2.
Gupta, V. K., O. J. Mesa, and D. R. Dawdy (1994), Multiscaling theory of flood peaks: Regional quantile analysis, *Water Resour. Res.*, *30*(12), 3405–3421, doi:10.1029/94WR01791.
Gupta, V. K., S. L. Castro and T. M. Over (1996), On scaling exponents of spatial peak flows from rainfall and river network geometry, *J. Hydrol.*, *187*, 81–104, doi:10.1016/S0022–1694(96)03088-0.
Halsey, T. C., M. H. Jensen, L. P. Kadanoff, I. Procaccia, and B. I. Shraiman (1986), Fractal measures and their singularities: The characterization of strange sets, *Phys. Rev. A Gen. Phys.*, *33*, 1141–1151, doi:10.1103/PhysRevA.33.1141.
Hollinger, S. E., J. R. Angel, and M. A. Palecki (2002), Spatial distribution, variation, and trends in storm precipitation characteristics associated with soil erosion in the United States, *Ill. State Water Survey Contract Rep. 2002-08*, 103 pp.
Hamon, W. R., (1961), Estimating potential evapotranspiration, *Transactions of the American Society of Civil Engineers*, *128*, 324–342.

Ishak, E. H., K. Haddad, M. Zaman, and A. Rahman (2011), Scaling property of regional floods in New South Wales Australia, *Nat. Hazards*, *58*(3), 1155–1167, doi:10.1007/s11069-011-9719-6.
Jensen, J. L. (1998), Some statistical properties of power averages of lognormal samples, *Water Resour. Res.*, *34*(9), 2415–2418, doi:10.1029/98WR01557.
Kroll, C. N., and P. Song (2013), Impact of multicollinearity on small sample hydrologic regression models, *Water Resour. Res.*, *49*, 3756–3769, doi:10.1002/wrcr.20315.
Modarres, R. (2010), Low flow scaling with respect to drainage area and precipitation in northern Iran, *J. Hydrol. Eng.*, *15*(3), 210–214, doi:10.1061/(ASCE)HE.1943–5584.0000181.
Ophori, D., and J. Tóth (1990), Relationships in regional groundwater discharge to streams: An analysis by numerical simulation, *J. Hydrol.*, *119*, 215–244, doi:10.1016/0022–1694(90)90044-X.
Over, T. M., and V. K. Gupta (1996), A space-time theory of mesoscale rainfall using random cascades, *J. Geophys. Res.*, *101*(D21), 26,319–26,331, doi:10.1029/96JD02033.
Over, T. M., J. D. Riley, J. B. Sharpe, and D. Arvin (2014), Estimation of regional flow-duration curves for Indiana and Illinois, *U.S. Geol. Surv. Sci. Invest. Rep., 2014–5177*, 24 pp.
Pandey, G. R. (1998), Assessment of scaling behavior of regional floods, *J. Hydrol. Eng.*, *3*(3), 169–173, doi:10.1061/(ASCE)1084-0699(1998)3:3(169).
Ries, K. G., III (2007), The national statistics program: A computer program for estimating streamflow statistics for ungaged sites, *U.S. Geol. Surv. Tech. Methods, 4-A6*, 37 pp.
Singh, K. P. (1971), Model flow duration and streamflow variability, *Water Resour. Res.*, *7*(4), 1031–1036, doi:10.1029/WR007i004p01031.
Skaugen, T., and T. Vaeringstad (2005), A methodology for regional flood frequency estimation based on scaling properties, *Hydrol. Processes*, *19*(7), 1481–1495, doi:10.1002/hyp.5588.
Smith, J. A. (1992), Representation of basin scale in flood peak distributions, *Water Resour. Res.*, *28*(11), 2993–2999, doi:10.1029/92WR01718.
Tasker, G. D., and J. R. Stedinger (1987), Regional regression of flood characteristics employing historical information, *J. Hydrol.*, *96*, 255–264.
Tessier, Y., S. Lovejoy, and D. Schertzer (1996), Multifractal analysis and modeling of rainfall and river flows and scaling, causal transfer functions, *J. Geophys. Res.*, *101*(D21), 26,427–26,440, doi:10.1029/96JD01799.
Tóth, J. (1963), A theoretical analysis of groundwater flow in small drainage basins, *J. Geophys. Res.*, *68*(16), 4795–4812, doi:10.1029/JZ068i016p04795.
Vogel, R. M. and N. M. Fennessey (1995), Flow duration curves II: A review of applications in water resources planning, *J. Am. Water Resour. Assoc.*, *31*(6), 1029–1039, doi:10.1111/j.1752-1688.1995.tb03419.x.
Vogel, R. M., and C. N. Kroll (1990), Generalized low-flow frequency relationships for ungauged sites in Massachusetts, *Water Resour. Bull.*, *26*, 241–253.
Vogel, R. M., and C. N. Kroll (1992), Regional geohydrologicgeomorphic relationships for the estimation of low-flow statistics, *Water Resour. Res.*, *28*(9), 2451–2458, doi:10.1029/92WR01007.
Vogel, R. M., and A. Sankarasubramanian (2000), Spatial scaling properties of annual streamflow in United States, *Hydrol. Sci.*, *45*(3), 465–476, doi:10.1080/02626660009492342.
Wolock, D. M., and G. J. McCabe (1995), Comparison of single and multiple flow-direction algorithms for computing topographic parameters in TOPMODEL, *Water Resources Research*, *31*, 1315–1324.
Wolman, M. G., and R. Gerson (1978), Relative scales of time and effectiveness of climate in watershed geomorphology, *Earth Surf. Processes*, *3*, 189–208.
Wooldridge, J. M. (2009), *Introductory Econometrics: A Modern Approach*, 4th ed., pp. 89–94. South-Western Cengage Learn., Mason, Ohio.
Wörman, A., A. I. Packman, L. Markland, J. W. Harvey, and S. H. Stone (2007), Fractal topography and subsurface water flows from fluvial bedforms to the continental shelf, *Geophys. Res. Lett.*, *34*, L07402, doi:10.1029/2007GL029426.
Yue, S., and T. Y. Gan (2004), Simple scaling properties of Canadian annual average streamflow, *Adv. Water Resour.*, *27*(5), 481–495, doi:10.1016/j.advwatres.2004.02.019.
Yue, S., and T. Y. Gan (2009), Scaling properties of Canadian flood flows, *Hydrol. Processes*, *23*(2), 245–258, doi:10.1002/hyp.7135.
Yue, S., and C. Y. Wang (2004), Scaling of Canadian low flows, *Stoch. Environ. Res. Risk Assess.*, *18*, 291–305, doi:10.1007/s00477-004-0176-6.